



# Characterization of atmospheric trace gases and particulate matter in Hangzhou, China

Gen Zhang<sup>1</sup>, Honghui Xu<sup>2</sup>, Bing Qi<sup>3</sup>, Rongguang Du<sup>3</sup>, Ke Gui<sup>1</sup>, Hongli Wang<sup>4</sup>, Wanting Jiang<sup>5</sup>, Linlin Liang<sup>1</sup>, and Wanyun Xu<sup>1</sup>

<sup>1</sup>State Key Laboratory of Severe Weather & Key Laboratory of Atmospheric Chemistry of CMA, Chinese Academy of Meteorological Sciences, Beijing 100081, China

<sup>2</sup>Zhejiang Institute of Meteorological Science, Hangzhou 310008, China

<sup>3</sup>Hangzhou Meteorological Bureau, Hangzhou 310051, China

<sup>4</sup>State Environmental Protection Key Laboratory of Formation and Prevention of Urban Air Pollution Complex, Shanghai Academy of Environmental Sciences, Shanghai 200233, China

<sup>5</sup>Plateau Atmospheric and Environment Laboratory of Sichuan Province, College of Atmospheric Science, Chengdu University of Information Technology, Chengdu 610225, China

**Correspondence:** Gen Zhang (zhanggen@cma.gov.cn) and Honghui Xu (forsnow@126.com)

Received: 21 August 2017 – Discussion started: 15 September 2017

Revised: 30 November 2017 – Accepted: 20 December 2017 – Published: 6 February 2018

**Abstract.** The Yangtze River Delta (YRD) is one of the most densely populated regions in China with severe air quality issues that have not been fully understood. Thus, in this study, based on 1-year (2013) continuous measurement at a National Reference Climatological Station (NRCS, 30.22° N, 120.17° E; 41.7 m a.s.l.) in the center of Hangzhou in the YRD, we investigated the seasonal characteristics, interspecies relationships, and the local emissions and the regional potential source contributions of trace gases (including O<sub>3</sub>, NO<sub>x</sub>, NO<sub>y</sub>, SO<sub>2</sub>, and CO) and particulate matter (PM<sub>2.5</sub> and PM<sub>10</sub>). Results revealed that severe two-tier air pollution (photochemical and haze pollution) occurred in this region, with frequent exceedances in O<sub>3</sub> (38 days) and PM<sub>2.5</sub> (62 days). O<sub>3</sub> and PM<sub>2.5</sub> both exhibited distinct seasonal variations with reversed patterns: O<sub>3</sub> reaching a maximum in warm seasons (May and July) but PM<sub>2.5</sub> reaching a maximum in cold seasons (November to January). The overall results from interspecies correlation indicated a strong local photochemistry favoring the O<sub>3</sub> production under a volatile organic compound (VOC)-limited regime, whereas it moved towards an optimum O<sub>3</sub> production zone during warm seasons, accompanied by the formation of secondary fine particulates under high O<sub>3</sub>. The emission maps of PM<sub>2.5</sub>, CO, NO<sub>x</sub>, and SO<sub>2</sub> demonstrated that local emissions were significant for these species on a seasonal scale. The contribu-

tions from the regional transport among inland cities (Zhejiang, Jiangsu, Anhui, and Jiangxi Province) on a seasonal scale were further confirmed to be crucial to air pollution at the NRCS site by using backward trajectory simulations. Air masses transported from the offshore areas of the Yellow Sea, East Sea, and South Sea were also found to be highly relevant to the elevated O<sub>3</sub> at the NRCS site through the analysis of potential source contribution function (PSCF). Case studies of photochemical pollution (O<sub>3</sub>) and haze (PM<sub>2.5</sub>) episodes both suggested the combined importance of local atmospheric photochemistry and synoptic conditions during the accumulation (related with anticyclones) and dilution process (related with cyclones). Apart from supplementing a general picture of the air pollution state in the city of Hangzhou in the YRD region, this study specifically elucidates the role of local emission and regional transport, and it interprets the physical and photochemical processes during haze and photochemical pollution episodes. Moreover, this work suggests that cross-regional control measures are crucial to improve air quality in the YRD region, and it further emphasizes the importance of local thermally induced circulation for air quality.

## 1 Introduction

Ambient air quality is mainly affected by particulate matter (PM<sub>2.5</sub> and PM<sub>10</sub>) and gaseous pollutants such as ozone (O<sub>3</sub>), nitrogen oxides (NO<sub>x</sub>), carbon monoxide (CO), and sulfur dioxide (SO<sub>2</sub>). Particulate matter comes from both natural sources (e.g., windborne dust, volcanoes) and anthropogenic activities such as fossil and biomass fuel combustion (Chow and Watson, 2002). In addition to the net downward transport of O<sub>3</sub> by eddy diffusion from the stratosphere aloft, tropospheric O<sub>3</sub> is a well-known secondary gaseous pollutant, and it is formed through the photochemical oxidation of volatile organic compounds (VOCs) and NO<sub>x</sub> under the irradiation of sunlight (Logan, 1985; Roelofs and Lelieveld, 1997). These chemicals have both received extensive attention either due to their harmful impact on human health (Pope and Dockery, 1999; Shao et al., 2006; Streets et al., 2007; Liu et al., 2013) and vegetation (Feng et al., 2014) or significant effects on climate change (Seinfeld et al., 2004; IPCC, 2007; Mercado et al., 2009). Moreover, some critical interactions have been verified to exist between the gaseous pollutants and/or particulate matter (Zhang et al., 2004; Cheng et al., 2016). For instance, in the presence of high NH<sub>3</sub> and low air temperature, ammonium nitrate (NH<sub>4</sub>NO<sub>3</sub>) is formed in regions with HNO<sub>3</sub> and NH<sub>3</sub>, which is an important constituent of PM<sub>2.5</sub> under high NO<sub>x</sub> conditions (Seinfeld and Pandis, 2006). To some extent, such interactions further improve or deteriorate the air quality. The oxidation of SO<sub>2</sub> leads to acid deposition but also contributes to the formation of sulfate aerosols (Meagher et al., 1978; Saxena and Seigneur, 1987), which in turn will influence the solar radiation and photochemistry (Dickerson et al., 1997) and further weaken the formation of secondary pollutants. Therefore, clear understanding of their characteristics, sources, transport, and formation mechanisms, including interactions, is crucial for gaining comprehensive information on complex air pollution.

The Yangtze River Delta (YRD) region is located in the east of China, and it includes the megacity of Shanghai and the well-industrialized areas of southern Jiangsu Province and northern Zhejiang Province, with over 10 large cities such as Hangzhou, Suzhou, Wuxi, and Changzhou lying along the mid-YRD (Fig. 1). Being one of the most rapidly growing regions in China in terms of transportation, industries, and urbanization, it has become a hot spot for air pollution over the past 3 decades, together with the Pearl River Delta (PRD) and Beijing–Tianjin–Hebei (BTH) regions. To date, numerous combined studies of O<sub>3</sub> and PM<sub>2.5</sub> were implemented in representative urban cities in the YRD region such as Shanghai (Geng et al., 2007; Ding et al., 2013; L. Li et al., 2016; Miao et al., 2017a) and Nanjing (Wang et al., 2002, 2003; Kang et al., 2013; Chen et al., 2016). On the contrary, in Hangzhou (29.25–30.5° N, 118.34–120.75° E), the capital city of Zhejiang Province in the YRD region, which lies along the mid-YRD, only a few sole studies of

PM<sub>2.5</sub> or O<sub>3</sub> have been sporadically conducted. PM<sub>2.5</sub> measurements in the city of Hangzhou have only been performed in the past 5 years, mostly covering a short-term period in winter (Jansen et al., 2014; Yu et al., 2014; Liu et al., 2015; J. Wu et al., 2016). Furthermore, there was still certain discrepancy about the origin of PM<sub>2.5</sub>. J. Wu et al. (2016) concluded that local vehicle emissions were a major contributor to PM<sub>2.5</sub>, while results from Yu et al. (2014) suggested that cross-border transport rather than local emissions control high PM<sub>2.5</sub> concentration and formation. Similarly, the photochemical pollution in the city of Hangzhou was also not well understood. To the best of our knowledge, the pioneer measurements of O<sub>3</sub> in or around Hangzhou started in the 1990s at the Lin'an site, a regional station located in the east of Zhejiang Province (50 km away from Hangzhou) (Luo et al., 2000). Subsequent studies at this site depicted the first picture of the seasonal variations of O<sub>3</sub> and its precursors (Wang et al., 2001, 2004). In the city of Hangzhou, only short-term measurements of O<sub>3</sub> were recently made during the summertime of 2013 (Li et al., 2017). Hence, there is a large knowledge gap concerning seasonal characteristics of these pollutants and a discrepancy in their origin; these are both crucial for fully understanding the complex combined pollution of PM<sub>2.5</sub> and O<sub>3</sub> in the city of Hangzhou.

To supplement the seasonal picture of air pollution in YRD, we conducted continuous measurements of trace gases (O<sub>3</sub>, NO<sub>x</sub>, NO<sub>y</sub>, CO, and SO<sub>2</sub>) and particulate matter (PM<sub>2.5</sub> and PM<sub>10</sub>) during January–December 2013 at a regional site, NRCS (National Reference Climatological Station), in Hangzhou, which is also an integrated measurement site for the research of climate change and the atmospheric environment. This study presents the first results of 1-year measurements of trace gases and particulate matter in the city of Hangzhou and investigates the characteristics and causes of these chemicals by discussing their seasonal characteristics, interspecies correlations, the concentration dependence on local emissions and regional transport, and specific photochemical pollution and haze cases.

## 2 Experiment and meteorological conditions

### 2.1 Site description

Hangzhou is situated on the eastern coast of China and is one of the most developed cities in the Yangtze River Delta region. It has a population of 8.9 million and an occurrence of 2.7 million vehicles according to the 2014 Statistical Bulletin of Hangzhou. It is categorized as being in a subtropical monsoon climate, with an average temperature of 17.0 °C, relative humidity of 75 %, and rainfall of 1438 mm over the past 30 years (1981–2010). In this study, all in situ measurements of gaseous constituents, particulates, and meteorological factors were conducted at a site named NRCS (30.22° N, 120.17° E; 41.7 m a.s.l.) in the center of Hangzhou (Fig. 1).

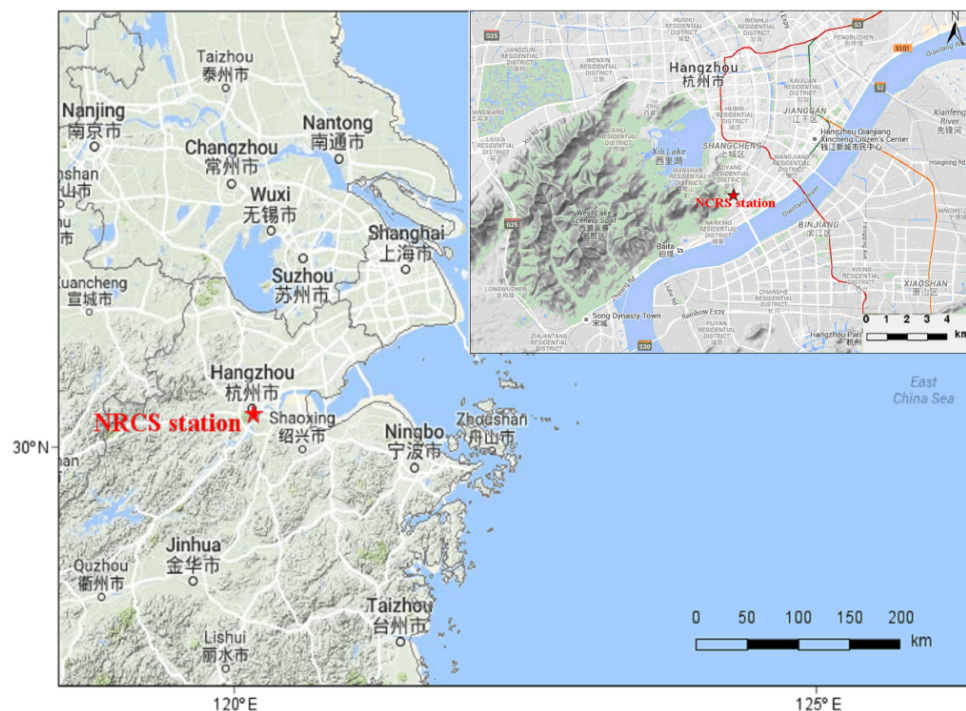


**Figure 1.** Location of the NRCS in the YRD region (left) and in the city of Hangzhou (top right).

As a typical urban site, the NRCS is situated in the commercial and residential areas in southern Hangzhou, and thus it is characterized as a polluted receptor site as it receives local urban plumes and regional air masses from the YRD region when northwesterly wind prevails. Moreover, as the map shows in the top right of Fig. 1, the site is adjacent to Prince Bay Park (area 0.8 km<sup>2</sup>) and is situated in the northeastern part of the famous scenic spot of West Lake (area 49 km<sup>2</sup>). Therefore it can also capture the signature of vegetation emission in the city of Hangzhou under southwestly winds. Moreover, there are no local industrial pollution sources around the site. In brief, this site can be representative of the city of Hangzhou.

## 2.2 Measurements' description

Measurements of trace gases, aerosols, and meteorological parameters were conducted at the NRCS during January–December 2013. Trace gases including O<sub>3</sub> and SO<sub>2</sub> were detected by a set of commercial trace gas analyzers (Thermo Environmental Instruments Inc., USA i-series 49i, 43i) with a resolution of 1 min. NO and NO<sub>x</sub> were detected by a chemiluminescence analyzer coupled with an internal MoO catalytic converter (TEI, 42i). Note that the differentiated value of NO<sub>2</sub> from NO<sub>x</sub> and NO represents the upper limit concentration of atmospheric NO<sub>2</sub> due to the interference of other nitrogen-containing components (e.g., PAN, HNO<sub>3</sub>, and HONO) in the conversion (Xu et al., 2013). Similar to NO<sub>x</sub>, NO<sub>y</sub> was also detected by a chemiluminescence ana-

lyzer (TEI 42i-Y) equipped with an external MoO catalytic converter. CO was monitored with a gas filter correlation infrared absorption analyzer (TEI, 48i), with automatic zeroing every 6 h. All the instruments are housed on the top floor of a laboratory building, which sits on the top of a hill about 40 m above ground level. Ambient air was drawn from the 1.5 m above the rooftop to the laboratory building through a manifold connected to O<sub>3</sub>, SO<sub>2</sub>, NO, and CO analyzers with PFA Teflon™ tubes (inside diameter: 2 cm). A separate sample line with a MoO converter was used for the NO<sub>y</sub> analyzer. All trace gas analyzers had a weekly span and were zero checked daily, except CO, and multi-point calibration was conducted once a month.

Ambient PM<sub>2.5</sub> samples were collected using co-located Thermo Scientific (formerly R&P) Model 1405D samplers. The sensor unit contains the two mass measurement hardware systems that monitor particulates that continuously accumulate on the system's exchangeable TEOM filters. Coarse PM and particulate PM<sub>2.5</sub>, split by a virtual impactor, each accumulate on the system's exchangeable TEOM filters. By maintaining a flow rate of 1.67 L min<sup>-1</sup> through the coarse sample flow channel and 3 L min<sup>-1</sup> through the PM<sub>2.5</sub> sample channel, and measuring the total mass accumulated on each of the TEOM filters, the device can calculate the mass concentration of both the PM<sub>2.5</sub> and coarse PM sample streams in near-real time. TEOM filters must be replaced before the filter loading percentage reaches 80 % to ensure the quality of the data generated by the instrument. For PM,

**Table 1.** Statistics of general meteorological parameters at NRCS for the period of January–December 2013\*.

Month	Temperature (°C)	RH (%)	Wind speed (m s <sup>-1</sup> )	Rainfall (mm)	Pressure (Pa)	Visibility (m)
January	4.5 ± 3.4	76 ± 9	1.9	24.9	10 221.6	2566
February	7.0 ± 4.3	81 ± 6	2.3	66.8	10 197.2	3512
March	12.3 ± 4.2	67 ± 15	2.7	115.9	10 140.5	5459
April	16.9 ± 3.9	56 ± 17	2.6	98.1	10 095.3	7588
May	23.0 ± 3.0	69 ± 13	2.1	121.3	10 045.8	6119
June	24.7 ± 3.1	78 ± 7	2.0	346	10 013.0	5694
July	32.3 ± 1.6	51 ± 7	2.8	9.3	9997.8	17 011
August	31.3 ± 2.7	58 ± 14	2.6	212.1	10 001.7	13 958
September	25.0 ± 2.7	73 ± 11	2.3	49.4	10 015.2	9585
October	19.3 ± 2.8	73 ± 11	2.5	331	10 146.1	7552
November	13.5 ± 3.9	68 ± 16	1.9	32.6	10 178.8	5759
December	6.3 ± 3.6	64 ± 15	2.0	82.7	10 208.6	3941

\* Note: average values for air temperature ( $T$ ), relative humidity (RH), wind speed (WS), accumulated monthly value of rainfall, pressure, and visibility.

the precisions of this instrument were  $2.0 \mu\text{g cm}^{-3}$  for a 1 h average and  $1.0 \mu\text{g cm}^{-3}$  for a 24 h average.

### 2.3 Meteorological characteristics

Table 1 shows the monthly averaged meteorological parameters at the NRCS, suggesting distinct characteristics of air temperature in winter and summer in this region, with monthly averages from ca.  $5^\circ\text{C}$  in January to ca.  $32^\circ\text{C}$  in July. High relative humidity (RH) and a large amount of rainfall appeared in June (346 mm in total), and oppositely less precipitation and low RH in autumn and winter. Note that the seemingly high RH and large rainfall that occurred in October was due to an extremely synoptic event on 7 October 2013 with total daily rainfall of 91 mm. In addition, the wind rose implied that the prevailing wind was from the northwest in autumn, the north in winter, and from the southwest in spring and summer (see Fig. S1v in the Supplement).

## 2.4 Methodology

### 2.4.1 Air mass back trajectory cluster

In this study, 72 h back trajectories starting at the arrival level of 100 m from NRCS sites were calculated by using the National Oceanic and Atmospheric Administration (NOAA) HYSPLIT-4 model with a  $1^\circ \times 1^\circ$  grid and the final meteorological database. The 6-hourly final archive data were obtained from the National Center for Environmental Prediction's Global Data Assimilation System (GDAS) wind field reanalysis. GDAS uses a spectral medium-range forecast model. More details can be found at <http://www.arl.noaa.gov/ready/open/hysplit4.html>. The model was run four times per day at starting times of 00:00, 06:00, 12:00, and 18:00 UTC (08:00, 14:00, 20:00, and 02:00 LT, respectively).

The method used in trajectory clustering was based on the GIS-based software TrajStat (Wang et al., 2004).

### 2.4.2 Potential source contribution function

The potential source contribution function (PSCF) is widely used to identify regional sources based on the HYSPLIT model. The zone of concern is divided into  $i \times j$  small equal grid cells. The PSCF value in the  $ij$ th cell is defined as  $m_{ij} / n_{ij}$ , where  $n_{ij}$  is denoted as the number of endpoints that fall in the  $ij$ th cell and  $m_{ij}$  represents the numbers of “polluted” trajectory endpoints in the  $ij$ th cell. In this analysis, average concentrations were considered to be the threshold of pollution (Hsu et al., 2003; Zhang et al., 2013). To minimize the effect of small values of  $n_{ij}$ , following the method of Polissar et al. (1999), the seasonal PSCF values were multiplied by arbitrary seasonal weight functions  $W_{ij}$ , expressed by WPSCF, to better reflect the uncertainty in the values for these cells. Geographic areas covered by more than 95 % of the back trajectories are selected as the study domain. In this study, our study domain was in the range of  $15\text{--}55^\circ\text{N}$  and  $105\text{--}135^\circ\text{E}$ . The resolution was  $0.5^\circ \times 0.5^\circ$ .

$$W_{ij(\text{spring})} = \begin{cases} 1.00 & 36 < n_{ij} \\ 0.70 & 12 < n_{ij} \leq 36 \\ 0.42 & 6 < n_{ij} \leq 12 \\ 0.17 & n_{ij} \leq 6 \end{cases}$$

$$W_{ij(\text{summer})} = \begin{cases} 1.00 & 42 < n_{ij} \\ 0.70 & 14 < n_{ij} \leq 42 \\ 0.42 & 7 < n_{ij} \leq 14 \\ 0.17 & n_{ij} \leq 7 \end{cases}$$

$$W_{ij(\text{autumn})} = \begin{cases} 1.00 & 36 < n_{ij} \\ 0.70 & 12 < n_{ij} \leq 36 \\ 0.42 & 6 < n_{ij} \leq 12 \\ 0.17 & n_{ij} \leq 6 \end{cases}$$

$$W_{ij(\text{winter})} = \begin{cases} 1.00 & 54 < n_{ij} \\ 0.70 & 18 < n_{ij} \leq 54 \\ 0.42 & 9 < n_{ij} \leq 18 \\ 0.17 & n_{ij} \leq 9 \end{cases}$$

Moreover, to better elucidate the local and regional contribution to pollutants concentrations, we further compared the WPSCF results with their corresponding emission inventories of PM<sub>2.5</sub>, CO, NO<sub>x</sub>, and SO<sub>2</sub> in 2013 provided by Peking University (<http://inventory.pku.edu.cn/>), which were estimated by using a bottom-up approach with 0.1° × 0.1° spatial resolution (Wang et al., 2013; Huang et al., 2014; Zhong et al., 2014).

### 2.4.3 Geopotential height (GH)

The geopotential height (GH) fields derived from the National Center for Environmental Prediction (NCEP) global Final (FNL) reanalysis (<http://rda.ucar.edu/datasets/ds083.2/>) are typically used to classify the synoptic types (Miao et al., 2017b). In this study, daily GH fields at the 925 hPa level from the NCEP-FNL reanalysis covering the region (100–135° E, 20–50° N) were classified into the prevailing synoptic types during photochemical pollution and haze episodes as discussed in Sect. 3.5. The NCEP-FNL reanalysis was produced from the Global Data Assimilation System, which continuously assimilates observations from the Global Telecommunication System and other sources. The NCEP-FNL reanalysis fields were on 1° × 1° grids with a 6 h resolution.

## 3 Results and discussion

### 3.1 Concentration levels

To evaluate the overall concentration level of gaseous and particulate pollution at NRCS, we selected a Grade II standard of the Chinese Ambient Air Quality Standards (CAAQS, GB 3095-2012), which was released in 2012 by the China State Council and implemented through the whole nation in 2016 (MEP, 2012). Inferred from the Grade II CAAQS for PM<sub>2.5</sub> (75 µg m<sup>-3</sup> for 24 h average) and PM<sub>10</sub> (150 µg m<sup>-3</sup> for 24 h average), 62 and 26 days of PM<sub>2.5</sub> and PM<sub>10</sub> exceedances with daily averages of 102.2 and 195.3 µg m<sup>-3</sup> were classified through the period, respectively, mostly occurring in winter. For O<sub>3</sub>, about 38 days exceedances (75 ppbv for daily maximum 8 h average for the Grade II CAAQS) in total were found during the whole period, mostly covering the period from May to September. This suggests that Hangzhou was suffering from heavy

haze and photochemical pollution in cold and warm seasons. Concerning SO<sub>2</sub>, the annual mean was 10.9 ppbv in this study, nearly half of the yearly mean of SO<sub>2</sub> Grade II CAAQS (21 ppbv). It was reasonably attributed to the powerful measure of the Chinese government to control the emission of SO<sub>2</sub> starting in 1990 (He et al., 2002; Qi et al., 2012). Table 2 summarizes a statistical analysis of these species and lists the comparison with the previous results in other typical regions in China. In general, with respect to all these chemicals, our results were generally comparable with those observed by other contemporaneous measurements in Hangzhou and the other cities in YRD. As expected, regional differences among YRD, PRD, and BTH could also be found, as illustrated in Table 2. For instance, observed PM<sub>2.5</sub>, PM<sub>10</sub>, and CO concentrations were higher in BTH than those in YRD and PRD through the comparison among provincial capital cities in China during 2011–2014 (Chai et al., 2014; Wang et al., 2014), which has been extrapolated to show more emissions from coal-based industries and coal and biomass-burning-based domestic home heating in BTH in winter (Zhang et al., 2012; Yang et al., 2013; Chai et al., 2014). Moreover, slight decreases in PM<sub>2.5</sub> and PM<sub>10</sub> at NRCS were both evidenced by their respective difference between 2013 and 2010–2011 (Table 2), coincident with the results derived from the satellite data and ground monitoring in China (Ma et al., 2016; Seltnerich, 2016). For NO<sub>y</sub>, only rough comparison was implemented due to very limited measurements executed in China. The yearly mean NO<sub>y</sub> concentration of 63.7 ppbv in this study was slightly higher than 54.6 ppbv in Beijing (Y. Wu et al., 2016). It is interesting to note that slightly higher NO<sub>y</sub> at NRCS possibly indicated more abundance of nitrogen oxides in Hangzhou. Additionally, the daytime mean concentrations were comparable with those at nighttime for PM<sub>2.5</sub> in nearly all seasons but were higher for O<sub>3</sub> due to the daily variations in solar radiation and air temperature; the reverse is true for CO, NO<sub>x</sub>, and NO<sub>y</sub>.

### 3.2 Seasonal characteristics

Figure 2 shows seasonal variations of atmospheric O<sub>3</sub> (a), CO (b), NO (c), NO<sub>x</sub> (d), NO<sub>y</sub> (e), O<sub>x</sub> (f), PM<sub>2.5</sub> (g), PM<sub>10</sub> (h), and SO<sub>2</sub> (i). Ozone exhibits a distinguished seasonal variation, with a broad peak in late spring and middle summer (a maximum in May and a secondary maximum in July) and a minimum in winter (November to January). Its observed behavior at NRCS is different from what has been disclosed in previous studies conducted in southern and northern China, such as a summer minimum and an autumn maximum of O<sub>3</sub> found in Hong Kong and an early summer (June) broad maximum recorded in Beijing (Ding et al., 2008; Lin et al., 2008, 2009; Xue et al., 2014b; Zhang et al., 2014; Sun et al., 2016). Recently, Ding et al. (2013) presented two peaks of O<sub>3</sub> appearing in summer (July) and early autumn (September) at the Xianlin site in the suburban area

**Table 2.** Mean species levels for different seasons and different times of day and comparisons with other previous data reported in typical regions in China. SD represents standard deviation.

Species	Areas	Location	Period	The whole day			Day time (08:00–17:00)			Nighttime (18:00–07:00)		
				Mean	SD	Max	Mean	SD	Max	Mean	SD	Max
PM <sub>2.5</sub> ( $\mu\text{g m}^{-3}$ )		This study	DJF	74.2	49.3	406.4	75.1	50.5	406.4	73.6	48.4	325.5
			MAM	47.1	26.2	201.1	47.7	26.6	201.1	46.7	25.9	154.0
			JJA	34.6	22.5	181	35.1	25.7	181.0	34.3	20.0	139.6
			SON	52.5	34.4	272.4	51.7	33.3	238.1	53.1	35.1	272.4
YRD	Xiacheng District, Hangzhou (Sep–Nov 2013) monthly mean: $69 \mu\text{g m}^{-3\text{a}}$ NRCS, Hangzhou (2012) annual mean: $50.0 \mu\text{g m}^{-3\text{b}}$ Hangzhou (Sep 2010–Nov 2011 during non-rain days) annual average: $106\text{--}131 \mu\text{g m}^{-3\text{c}}$ Nine sites in Nanjing (2013) AM: $55\text{--}60 \mu\text{g m}^{-3}$ , JJA: $30\text{--}60 \mu\text{g m}^{-3}$ , SON: $55\text{--}85 \mu\text{g m}^{-3\text{d}}$ Nanjing (Mar 2013–Feb 2014) annual mean: $75 \pm 50 \mu\text{g m}^{-3\text{e}}$ Shanghai (Mar 2013–Feb 2014) annual mean: $56 \pm 41 \mu\text{g m}^{-3\text{e}}$											
BTH	Beijing (Mar 2013–Feb 2014) annual mean: $87 \pm 67 \mu\text{g m}^{-3\text{e}}$											
PRD	Guangzhou (Mar 2013–Feb 2014) annual mean: $52 \pm 28 \mu\text{g m}^{-3\text{e}}$											
PM <sub>10</sub> ( $\mu\text{g m}^{-3}$ )		This study	DJF	113.1	71.7	589.6	115.3	73.6	589.6	111.5	70.4	481.6
			MAM	77.1	42.3	484.1	79.3	41.0	249.1	75.6	43.2	484.1
			JJA	54.9	31.6	231.4	55.7	34.8	231.4	54.4	29.2	183.8
			SON	85.6	51.2	344.2	84.8	48.6	341.3	86.1	53.0	344.2
YRD	Hangzhou (Mar 2013–Feb 2014) annual mean: $98 \pm 59 \mu\text{g m}^{-3\text{e}}$ Hangzhou (Sep 2010–Nov 2011 during non-rain days) annual average: $127\text{--}158 \mu\text{g m}^{-3\text{c}}$ Hangzhou (Sep 2001–Aug 2002) annual mean: $119.2 \mu\text{g m}^{-3\text{f}}$ Nanjing (Mar 2013–Feb 2014) annual mean: $134 \pm 73 \mu\text{g m}^{-3\text{e}}$ Shanghai (Mar 2013–Feb 2014) annual mean: $80 \pm 47 \mu\text{g m}^{-3\text{e}}$											
BTH	Beijing (Mar 2013–Feb 2014) annual mean: $109 \pm 62 \mu\text{g m}^{-3\text{e}}$											
PRD	Guangzhou (Mar 2013–Feb 2014) annual mean: $72 \pm 35 \mu\text{g m}^{-3\text{e}}$											
O <sub>3</sub> (ppbv)		This study	DJF	13.8	13.1	70.9	17.7	14.1	70.9	10.2	10.9	58.5
			MAM	29.8	24.0	141.2	42.4	27.3	141.2	20.0	15.1	105.9
			JJA	31.3	26.0	145.4	48.8	26.6	145.4	18.2	15.8	118.7
			SON	25.9	22.5	100.1	37.0	25.1	100.1	16.3	14.3	99.5
YRD	Hangzhou (Mar 2013–Feb 2014) annual mean: $44 \pm 21 \text{ ppbv}$ (8 h O <sub>3</sub> ) <sup>e</sup> Nanjing (Mar 2013–Feb 2014) annual mean: $42 \pm 20 \text{ ppbv}$ (8 h O <sub>3</sub> ) <sup>e</sup> Shanghai (Mar 2013–Feb 2014) annual mean: $48 \pm 21 \text{ ppbv}$ (8 h O <sub>3</sub> ) <sup>e</sup>											
BTH	Beijing (Mar 2013–Feb 2014) annual mean: $45 \pm 27 \text{ ppbv}$ (8 h O <sub>3</sub> ) <sup>e</sup>											
PRD	Guangzhou (Mar 2013–Feb 2014) annual mean: $45 \pm 24 \text{ ppbv}$ (8 h O <sub>3</sub> ) <sup>e</sup>											
SO <sub>2</sub> (ppbv)		This study	DJF	14.5	10.2	71.2	16.2	10.2	71.2	13.3	10.2	64.6
			MAM	11.3	9.1	75.1	11.7	9.6	75.1	11.0	8.7	59.3
			JJA	8.6	6.5	51.0	8.0	6.3	51.0	9.0	6.6	46.7
			SON	9.6	7.2	63.8	10.3	7.1	58.3	9.0	7.3	63.8
YRD	Hangzhou Xiacheng District (12–19 Oct 2013) daily mean: $5.7\text{--}9.7 \text{ ppbv}^{\text{a}}$ Hangzhou (Mar 2013–Feb 2014) annual mean: $9 \pm 4 \text{ ppbv}^{\text{e}}$ Nanjing (Mar 2013–Feb 2014) annual mean: $12 \pm 6 \text{ ppbv}^{\text{e}}$ Shanghai (Mar 2013–Feb 2014) annual mean: $7 \pm 5 \text{ ppbv}^{\text{e}}$											
BTH	Beijing (Mar 2013–Feb 2014) annual mean: $9 \pm 8 \text{ ppbv}^{\text{e}}$											
PRD	Guangzhou (Mar 2013–Feb 2014) annual mean: $7 \pm 3 \text{ ppbv}^{\text{e}}$											

Table 2. Continued.

Species	Areas	Location	Period	The whole day			Day time (08:00–17:00)			Nighttime (18:00–07:00)		
				Mean	SD	Max	Mean	SD	Max	Mean	SD	Max
CO (ppmv)	YRD	This study	DJF	1.4	0.7	3.8	1.4	0.7	3.3	1.4	0.7	3.8
			MAM	0.7	0.2	2.2	0.7	0.3	2.2	0.7	0.2	1.7
			JJA	0.5	0.2	2.0	0.5	0.2	1.9	0.5	0.2	2.0
			SON	0.8	0.3	3.4	0.7	0.3	1.9	0.8	0.3	3.4
	Hangzhou (Mar 2013–Feb 2014) annual mean: $0.7 \pm 0.3$ ppmv <sup>e</sup> Nanjing (Mar 2013–Feb 2014) annual mean: $0.8 \pm 0.4$ ppmv <sup>e</sup> Shanghai (Mar 2013–Feb 2014) annual mean: $0.7 \pm 0.3$ ppmv <sup>e</sup>											
BTH	Beijing (Mar 2013–Feb 2014) annual mean: $1.1 \pm 0.7$ ppmv <sup>e</sup>											
PRD	Guangzhou (Mar 2013–Feb 2014) annual mean: $0.8 \pm 0.2$ ppmv <sup>e</sup>											
NO <sub>2</sub> (ppbv)	YRD	This study	DJF	37.4	20.1	146.9	35.7	19.5	126.3	38.5	20.5	146.9
			MAM	28.7	12.9	94.8	25.3	12.1	94.8	31.0	12.9	87.4
			JJA	17.3	10.2	61.4	13.0	9.2	46.1	20.3	9.7	61.4
			SON	28.4	15.2	94.1	25.1	13.3	86.2	30.7	16.0	94.1
	Hangzhou (Mar 2013–Feb 2014) annual mean: $13 \pm 9$ ppbv <sup>e</sup> Nanjing (Mar 2013–Feb 2014) annual mean: $26 \pm 11$ ppbv <sup>e</sup> Shanghai (Mar 2013–Feb 2014) annual mean: $20 \pm 9$ ppbv <sup>e</sup>											
BTH	Beijing (Mar 2013–Feb 2014) annual mean: $25 \pm 11$ ppbv <sup>e</sup>											
PRD	Guangzhou (Mar 2013–Feb 2014) annual mean: $24 \pm 10$ ppbv <sup>e</sup>											
NO <sub>x</sub> (ppbv)	YRD	This study	DJF	60.5	34.7	199.8	58.0	32.1	168.9	62.3	36.3	199.8
			MAM	40.0	19.8	131.4	36.5	19.2	129.2	42.5	19.8	131.4
			JJA	24.3	14.8	99.6	18.6	14.1	99.6	28.2	14.0	83.1
			SON	41.0	24.3	153.4	36.6	21.1	123.7	44.2	25.8	153.4
NO <sub>y</sub> (ppbv)	YRD	This study	DJF	84.7	48.4	295.2	82.4	44.6	263.7	86.4	51.1	295.2
			MAM	66.0	33.6	248.8	62.9	34.6	248.8	68.2	32.8	204.1
			JJA	43.6	27.6	259.5	36.8	29.3	259.5	48.5	25.2	167.7
			SON	70.2	37.9	319.3	65.5	35.6	319.3	73.6	39.1	251.8
Nanjing SORPES 2013 monthly mean: 30–70 ppbv <sup>g</sup> Shanghai May–June 2005 daily mean: 24–39 ppbv <sup>h</sup>												
BTH	Beijing 2011–2015 annual mean: $54.6 \pm 4.7$ ppbv <sup>a</sup>											
YRD	Guangzhou Apr–May 2004: 24–52 ppbv <sup>h</sup>											

<sup>a</sup> J. Wu et al. (2016). <sup>b</sup> Qi et al. (2015). <sup>c</sup> Sun et al. (2013). <sup>d</sup> Chen et al. (2016). <sup>e</sup> Wang et al. (2014). <sup>f</sup> Cao et al. (2009). <sup>g</sup> Ding et al. (2013). <sup>h</sup> Xue et al. (2014a).

northeast of Nanjing (about 239 km away from the NRCS). Regarding the geographical location of Hangzhou, which is upwind of the YRD under the influence of the southeasterly summer monsoon, the emissions in the YRD region and the solar radiation might be the main causes of an O<sub>3</sub> formation in summer, resulting in a different seasonal cycle of O<sub>3</sub> compared to other continent sites in the west/northwest of the YRD. In fact, the CO and NO<sub>y</sub> data (Fig. 2b and e) show that these precursors were still at fairly high levels (about 500 and 35 ppbv, respectively) in summer. The low O<sub>3</sub> level in winter, especially at night, can be attributed to the lower temperature, weaker solar radiation, and in particular the strong destruction of O<sub>3</sub> by chemical titration of NO from local emissions

or regional transport as discussed below (Lin et al., 2008, 2009, 2011). Note that a slight drop of O<sub>3</sub> was found in June compared with other months in summer, mainly attributed to the more frequent rainy days (23 days) and larger rainfall in June (346 mm) than those in May (15 days) and July (5 days) during summertime (Table 1).

For PM<sub>2.5</sub> and PM<sub>10</sub>, Fig. 2g and h both display overall well-defined seasonal variations with the maximum in winter (December) and the minimum in summer (July). In cold seasons the emission of particulate matter is normally high due to more emission of fossil fuels because of heating in northern China (Zhang et al., 2009), which contributed to the enhancement of particulate matter and other tracer gases

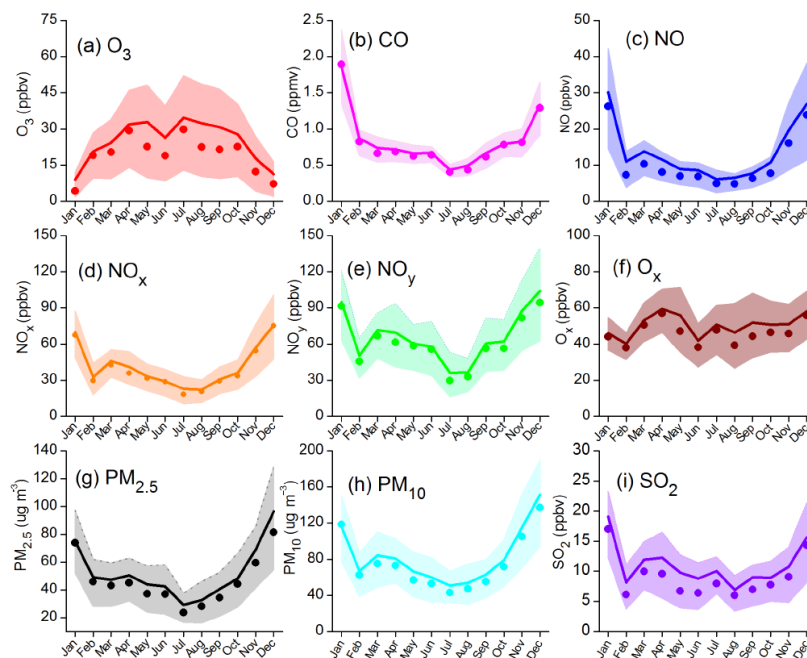


**Figure 2.** Seasonal variations of atmospheric O<sub>3</sub> (a), CO (b), NO (c), NO<sub>x</sub> (d), NO<sub>y</sub> (e), O<sub>x</sub> (f), PM<sub>2.5</sub> (g), PM<sub>10</sub> (h), and SO<sub>2</sub> (i). Bold solid lines show the monthly averages, solid circles show the median values, and thin lines represent percentiles of 75 and 25 %.

(i.e., CO and NO<sub>x</sub>) at the NRCS site via long-distance transport (see discussion in Sect. 3.4). Furthermore, in winter, temperature inversion and low mixing layer contribute to a decrease in particulate suspension and advection (Miao et al., 2015a). Also, dry/wet deposition should have strong seasonal variations because high precipitation favors wet deposition and high soil humidity, and the growth of deciduous plants may also favor the dry deposition of particulate matter in warm seasons (Zhang et al., 2001). The relatively low concentrations of PM<sub>2.5</sub> and PM<sub>10</sub> in summer may also be partly due to an increased vertical mixing (i.e., a higher boundary layer height) and more convection (Ding et al., 2013; Miao et al., 2015b). PM<sub>2.5</sub> mass concentration also shows strong month-to-month variations. The simultaneous drop of PM<sub>2.5</sub> and PM<sub>10</sub> concentrations together with other primary pollutants (i.e., SO<sub>2</sub>, CO and NO<sub>y</sub>) in February was mainly ascribed to the winter break of the Chinese Spring Festival, which started at the end of January and lasted until mid-February. Notably, the seasonal pattern for PM was similar to NO<sub>x</sub>, which suggested that traffic and heating emissions were important to the PM<sub>2.5</sub> variation.

Other trace gases (CO, NO<sub>x</sub>, NO<sub>y</sub>, and SO<sub>2</sub>) all revealed clear seasonal variations but also some unique month-to-month variation patterns (Fig. 2a–f and i). Similar seasonal patterns among CO, NO<sub>x</sub>, and SO<sub>2</sub> were generally found, with pronounced minimums appearing in summer and higher levels in autumn and winter. Similar reasons to particulate matter could interpret these seasonal patterns, such as the variation in the boundary layer height and the long-distance

transport as mentioned above. Last but not least was the photochemistry. During summer, it is most active, accelerating the transformation of primary gaseous pollutants, whereas in winter, a weaker photochemical reaction cannot remove the gases as quickly as in the warmer seasons from the atmosphere.

NO<sub>y</sub> concentration increased at the end of autumn, with a maximum in December together with a sharp peak of NO. The time series implied that in December there was a multi-day episode of NO<sub>x</sub> with high mixing ratios of NO and NO<sub>2</sub>, both reaching up to 100 ppbv, and these days were generally correlated with northwesterly wind, suggesting fresh emissions from factories in the industrial zone in the northwest. The potential ozone, O<sub>x</sub> (O<sub>3</sub> + NO<sub>2</sub>), is usually used as an estimate of atmospheric total oxidant (Lin et al., 2008). In winter (Fig. 2f), an abnormally high level of O<sub>x</sub> was found. The high level of NO<sub>2</sub> in O<sub>x</sub> was expected to be originated from the significant titration of high NO by O<sub>3</sub> in November and December (Fig. 2a).

As shown in Fig. 2i, SO<sub>2</sub> displayed a strong increase in winter but a significant drop in November. This pronounced winter peak was mainly due to the increased coal consumption for heating as mentioned above. The drop was associated with the PM<sub>2.5</sub> maximum and a relatively high RH (Fig. 2g and Table 1), suggesting a possible role of heterogeneous reactions (Ravishankara, 1997).

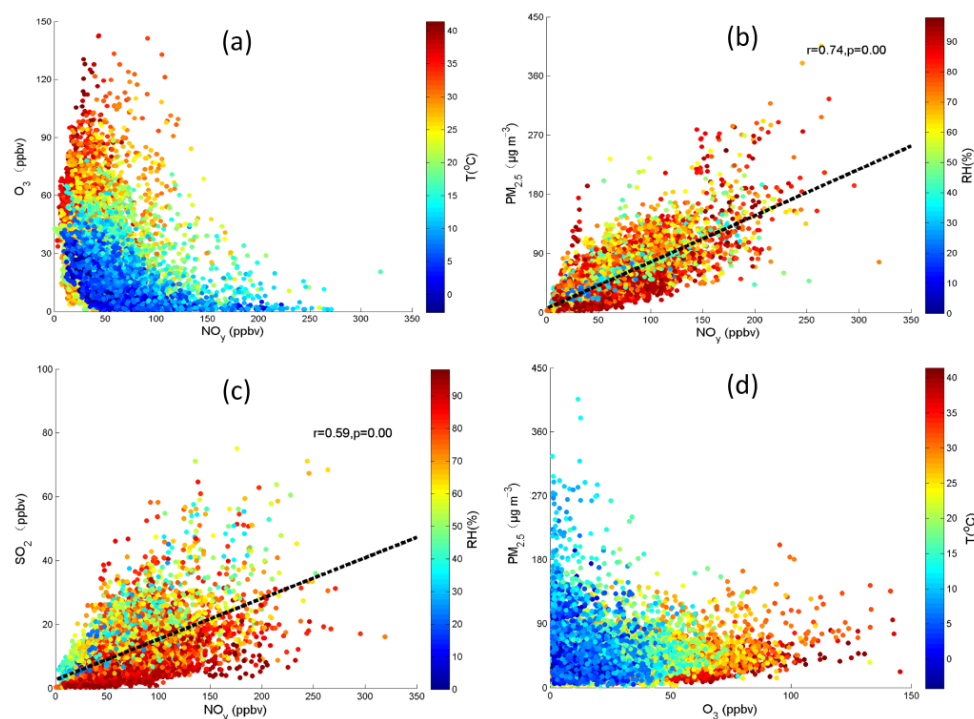


**Figure 3.** Scatter plots of  $\text{NO}_y$  with  $\text{O}_3$  ( $\text{NO}_y$ – $\text{O}_3$ ) color-coded with air temperature (a),  $\text{NO}_y$ – $\text{PM}_{2.5}$  color-coded with relative humidity (b),  $\text{NO}_y$ – $\text{SO}_2$  color-coded with relative humidity (c), and  $\text{O}_3$ – $\text{PM}_{2.5}$  color-coded with air temperature (d).

### 3.3 Interspecies correlations

Interspecies correlation can normally be used as a way to acquire some insights on their chemical formation, removal processes, and interactions. As displayed in Figs. 3 and 4, we present scatter plots of  $\text{NO}_y$ – $\text{O}_3$ ,  $\text{NO}_y$ – $\text{PM}_{2.5}$ ,  $\text{NO}_y$ – $\text{SO}_2$ ,  $\text{O}_3$ – $\text{PM}_{2.5}$ , and  $\text{NO}_y$ –CO correlations based on the whole dataset, and we further differentiate these correlations under typical environmental or meteorological impacts with color-coded parameters (i.e., relative humidity, air temperature, and  $\text{O}_3$  concentration). Clearly, an overall negative correlation was found between  $\text{O}_3$  and  $\text{NO}_y$  during the whole period (Fig. 3a). The color data showed that a negative correlation mainly appeared with data of low air temperature, implying a high titration of freshly emitted NO with  $\text{O}_3$  during the cold seasons and at nighttime. In contrast, a positive correlation between  $\text{O}_3$  and  $\text{NO}_y$  dominated under high air temperature, which usually occurred in the daytime of warm seasons within a moderate level of  $\text{NO}_y$  ( $< 150$  ppbv). These findings suggested a strong local photochemical production of  $\text{O}_3$  in summer, leading to its seasonal variations as illustrated in Fig. 2a.

As illustrated in Fig. 3b, a good positive correlation was found between  $\text{PM}_{2.5}$  and  $\text{NO}_y$ , suggesting that  $\text{PM}_{2.5}$  was highly correlated with fossil combustion at this site. Some green data in the plot show very high  $\text{NO}_y$  concentration together with low  $\text{PM}_{2.5}$ , suggesting that the concentration of

NO air masses is high during December. Figure 3b shows that high RH data were very scattered but  $\text{PM}_{2.5} / \text{NO}_y$  data were not, implying a negligible interference of humidity on TEOM  $\text{PM}_{2.5}$  measurement during the study period, even under high RH conditions in summer.

$\text{SO}_2$  and  $\text{NO}_y$  show a moderate to good correlation (see Fig. 3c). Specifically, a better correlation and higher  $\text{SO}_2 / \text{NO}_y$  ratio were gained from air with low humidity. Nevertheless, the point distribution was much more scattered for the humid air masses, and the ratio of  $\text{SO}_2 / \text{NO}_y$  was clearly low, confirming a higher conversion of  $\text{SO}_2$  to sulfate and/or deposition in humid conditions (Khoder, 2002; Su et al., 2011). In this study, the averaged ratio of  $\text{SO}_2 / \text{NO}_y$  during 18 February–30 April was 0.017, which is lower compared with that previously reported at Lin’an during the same months 12 years ago (Wang et al., 2004). This is mainly owed to a great reduction in  $\text{SO}_2$  emission from power plants but an increased  $\text{NO}_x$  emission associated with a huge consumption of petroleum fuels in the past decade in this region (Zhang et al., 2009).

A scatter plot of  $\text{O}_3$  with  $\text{PM}_{2.5}$  color-coded with air temperature is depicted in Fig. 3d. During periods of moderate to high air temperature, a significant positive correlation was elucidated between  $\text{O}_3$  and  $\text{PM}_{2.5}$ , and the reverse negative correlation was found under low temperatures. The positive correlation for warm air might reflect a formation of secondary fine particulates in summer associated with high

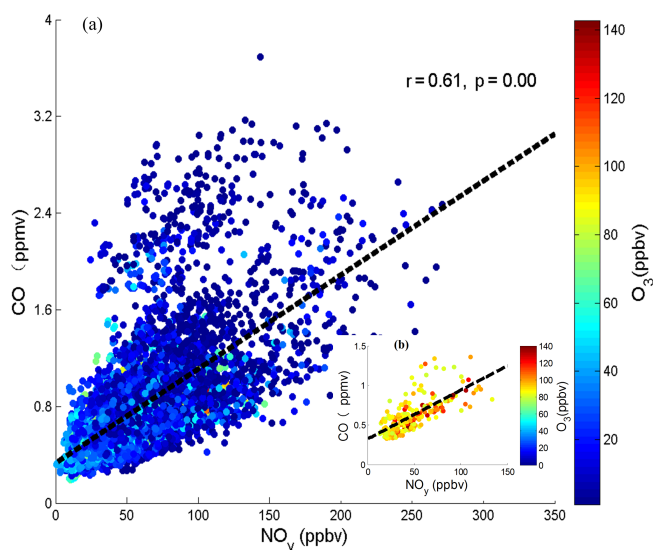


**Figure 4.** (a) Scatter plots of  $\text{NO}_y$  with CO color-coded with  $\text{O}_3$  mixing ratios are shown, as well as the inset (b) showing the scatter plot with  $\text{O}_3$  mixing ratios above 80 ppbv.

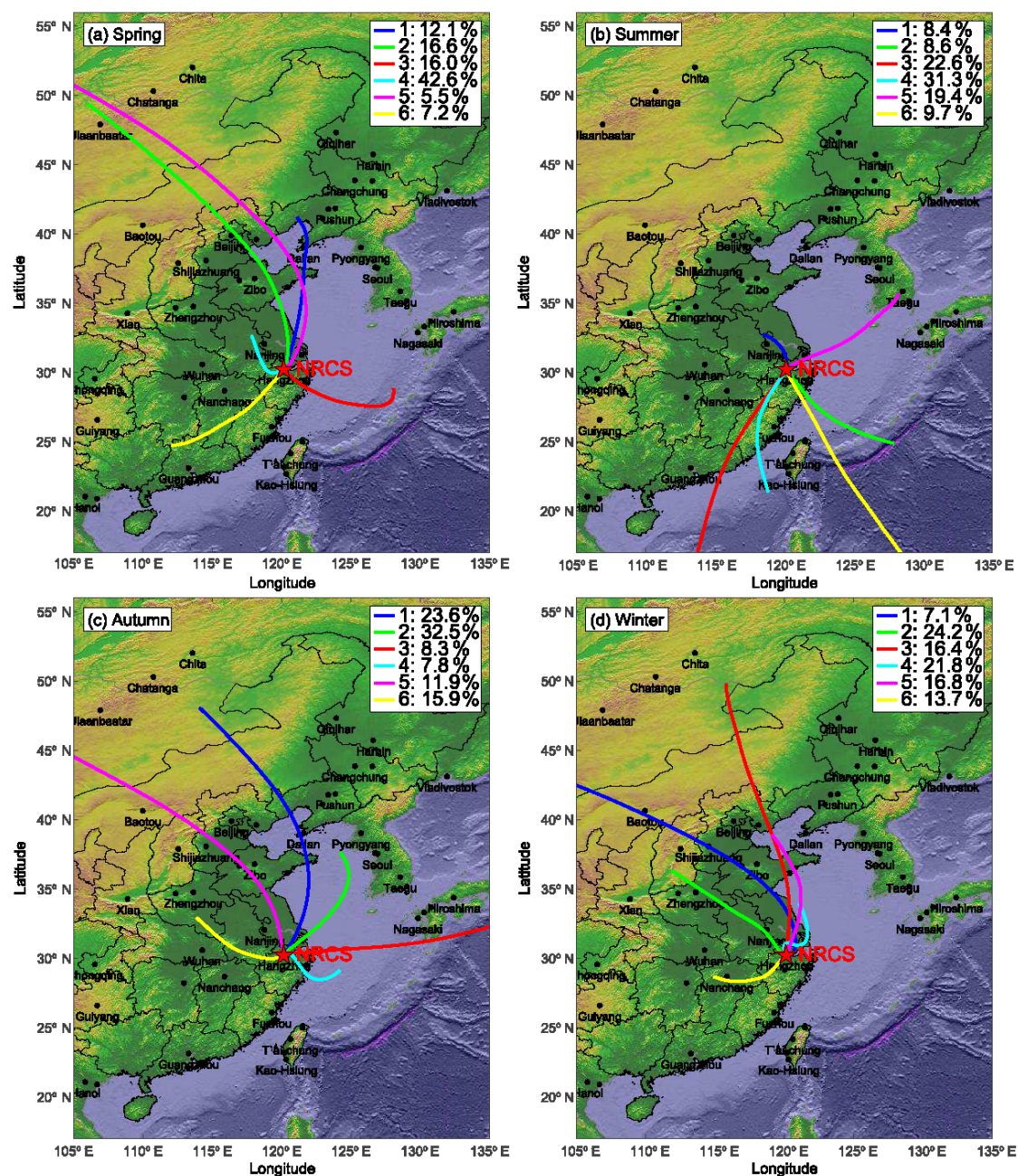
$\text{O}_3$ , which was confirmed by our comparison of the ratio of the averaged  $\text{PM}_{2.5}$  concentrations in the typical  $\text{O}_3$  exceedances events (OE) to that in nearby non- $\text{O}_3$  exceedances (NOE) events ( $\text{PM}_{2.5(\text{OE})} / \text{PM}_{2.5(\text{NOE})}$ ) with the ratios for other gaseous pollutants (Table S1 in the Supplement). The secondary particulate formation may be related to a high conversion rate of  $\text{SO}_2$  and  $\text{NO}_x$  to sulfate and nitrate under a high concentration of oxidants (Khoder, 2002; Sun et al., 2013). Additionally, it was also associated with the formation of secondary organic aerosols with high  $\text{O}_3$  concentrations (Kamens et al., 1999; Lambe et al., 2015; Palm et al., 2017), which were primarily produced through the photo-oxidation of BVOCs (Claeys, et al., 2004; Böge et al., 2013). As inferred above, significant emission of BVOCs was speculated around NRCS in summer. Note that it is necessary to implement more detailed investigations related with chemical elements, ion, and organic and elemental carbon (OC/EC) analysis of particulate matter. The anti-correlation for cold air might be caused by the titration effect of high NO concentration in relation to high primary  $\text{PM}_{2.5}$  in cold seasons, which was also reflected by the consistency of the seasonal variations in NO and  $\text{PM}_{2.5}$ .

Figure 4 shows a good positive correlation between CO and  $\text{NO}_y$  color-coded with  $\text{O}_3$  mixing ratios. For CO lower than 3.2 ppmv during the whole period, an increase of  $\text{NO}_y$  generally led to lower  $\text{O}_3$  concentrations, but CO showed a reverse pattern. As VOCs and CO have a common origin, VOCs show a similar behavior to CO in the ozone photochemistry in typical urban regions (Atkinson, 2000; Guo et al., 2004). Our results suggested a VOC-limited regime throughout the year in Hangzhou, consistent with the results reported in other cities of the YRD region (e.g., Shanghai and

Nanjing) (Geng et al., 2007; Ding et al., 2013). As specifically shown in Fig. 4b, atmospheric  $\text{O}_3$  (above 80 ppbv) mainly occurred in the afternoon (14:00–16:00 LT) in the summer and early autumn, exhibiting an increased trend with the increasing  $\text{NO}_y$  within air masses, with a moderate CO mixing ratio of 0.25–1.5 ppmv, and the reverse trend for CO was not expected to be significantly increased. This indicated that the transition from a VOC-limited regime to an optimum  $\text{O}_3$  production zone (even  $\text{NO}_x$ -limited regime) probably occurred at the NRCS site in warmer seasons. We speculated that this change was mainly attributed to the larger emission of biogenic VOCs (BVOCs) compared to cold seasons. As reviewed by Calafapietra et al. (2013), the VOC-limited conditions, in which  $\text{O}_3$  production is limited by a high concentration of  $\text{NO}_x$ , are often observed in urban areas. However, if high BVOC emitters are common in urban areas, they could move the VOC /  $\text{NO}_x$  ratio toward optimal values for  $\text{O}_3$  formation, resulting in this ratio being reached in the city centers. As depicted in Sect. 2.1, our study site is situated adjacent to Prince Bay Park (area 0.8 km<sup>2</sup>) and in the north-eastern part of the famous scenic spot of West Lake (area 49 km<sup>2</sup>). These two regions were both urban green parks with high vegetation coverage. Moreover, the primary tree species in these two regions, *Liquidambar formosana* and *Cinnamomum camphora*, respectively, are the major contributors to the emissions of isoprene and monoterpene (Chang et al., 2012), favoring the formation of  $\text{O}_3$ . Air masses from Prince Bay Park and West Lake famous scenic spot were confirmed to be transported to the NRCS site during warmer seasons, as illustrated in Figs. S1 and 8b. In view of the strong temperature dependence of isoprenoid emission (Guenther et al., 1995), a significantly increased emission of BVOCs was expected in warm seasons, and thus it disturbed the original balance between VOCs and  $\text{NO}_x$  relative to cold seasons. Our conclusion was generally in line with the contemporaneous study implemented by L. Li et al. (2016), who found that a VOC-limited regime accounted for 47 % of the ozone formation during the summer in Hangzhou and that the others are under a  $\text{NO}_x$ -limited regime, taking BVOCs into consideration. Recently, Li et al. (2017) also deduced that the summer ozone mostly presented a VOC-limited regime and a transition region alternately in the city of Hangzhou.

### 3.4 Dependences of pollutant concentrations on local emission and regional transport

To obtain an overview of the impact of wind on the pollutants' concentrations, we draw the seasonal wind dependence maps of pollutants' concentrations with wind sectors (see Fig. S2 for details). In total, similar seasonal patterns of the wind dependence map were found between CO and  $\text{PM}_{2.5}$ ,  $\text{SO}_2$ , and  $\text{NO}_y$  ( $\text{NO}_x$ ), in good agreement with their seasonal patterns as shown in Sect. 3.2. For CO and  $\text{PM}_{2.5}$ , their top 10 % concentrations were generally related with all the directions throughout the year at speeds lower than  $2 \text{ m s}^{-1}$ , while



**Figure 5.** Seasonal cluster analysis of the 72 h air mass back trajectories starting at 100 m from the NRCS site in Hangzhou.

their bottom 10 % were associated with other directions of wind, except northerly, at higher wind speeds. It is necessary to pay attention to the scatter points of the top 10 % of concentrations distributed in a northerly direction with high wind speed. With respect to the wind direction and transport, as the wind speed increases, pollutants' concentrations should have been decreasing due to the more effective local dilution, thus the increase instead might indicate potential sources in these directions.

To address this issue and further investigate the relative contribution of local emission and regional transport, we employed the trajectory clustering and WPSCF, along with the comparison with the emission inventories. The 72 h back trajectories from the NRCS site were computed using the HYSPLIT model for four seasons. As shown in Fig. 5, we obtained six clusters using the clustering algorithm for four seasons with seven dominant paths distributed in the east (E), northeast (NE), north (N), northwest (NW), west (W), south-

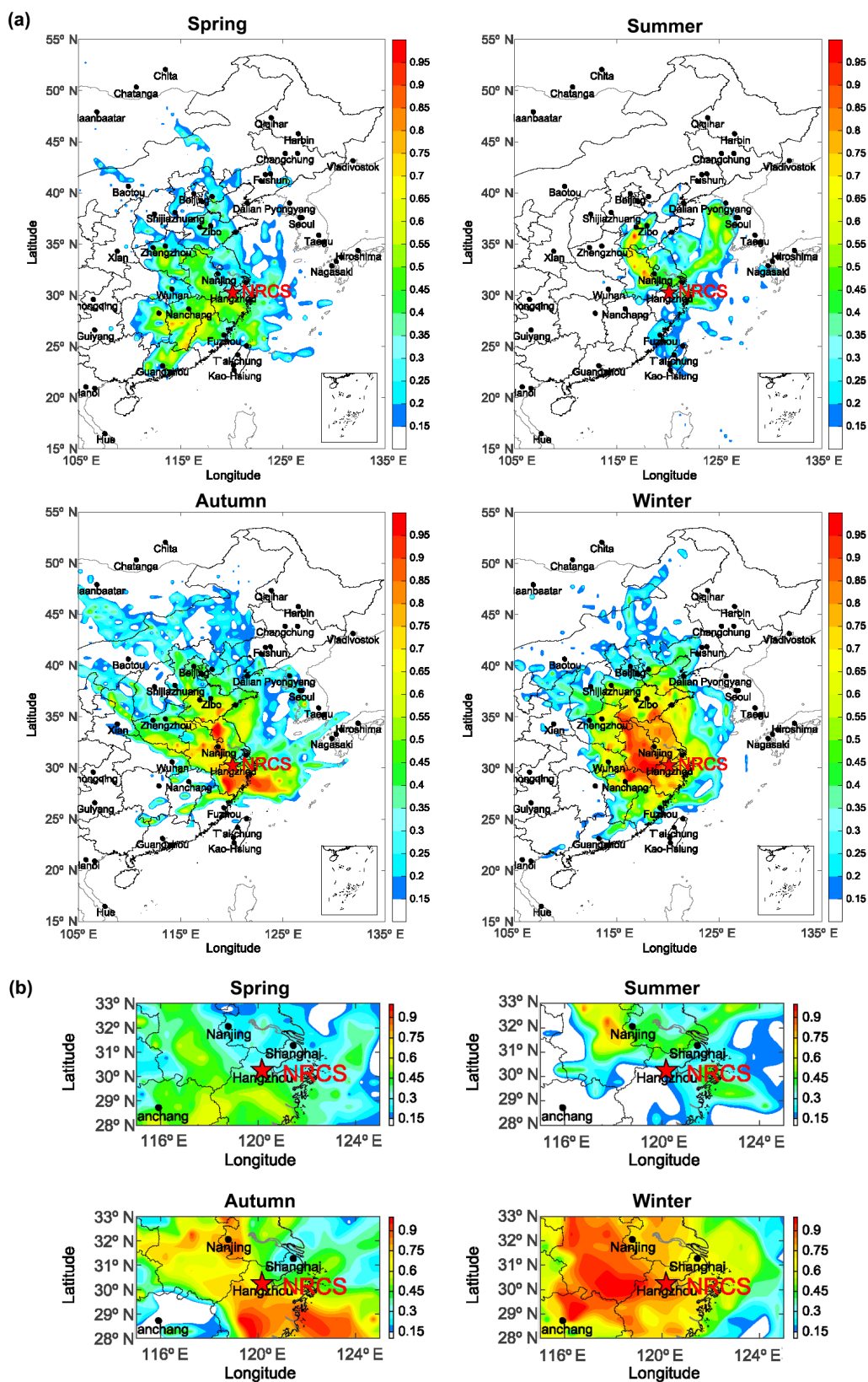
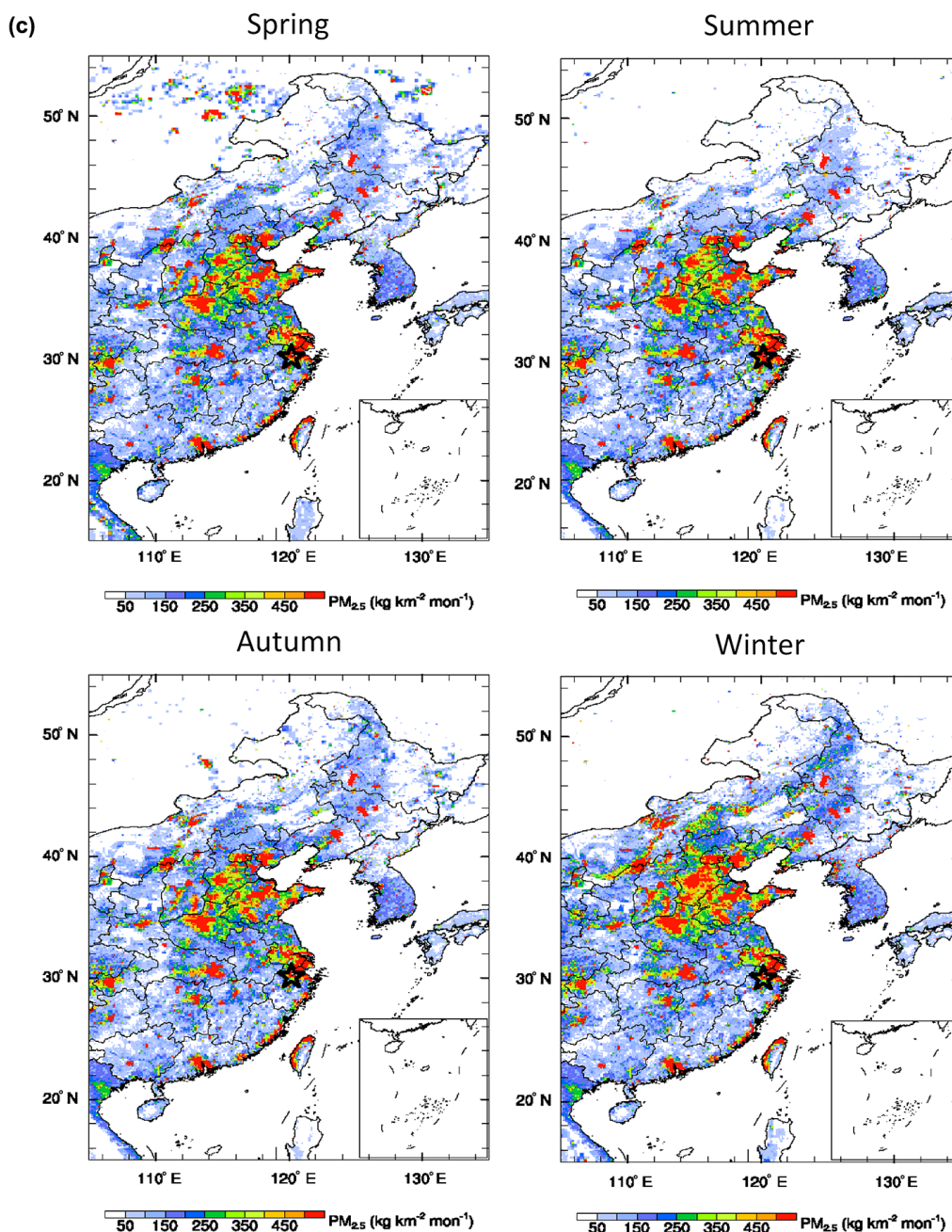


Figure 6.



**Figure 6.** (a) Seasonal weighted potential source contribution function (WPSCF) maps of  $\text{PM}_{2.5}$  in Hangzhou. The sampling site is marked by the star and the WPSCF values are displayed in color. (b) The zoomed view of Fig. 6a. (c) Seasonal and spatial distributions of  $\text{PM}_{2.5}$  emissions ( $\text{kg km}^2 \text{mon}^{-1}$ ) at the surface layer in China. The sampling site is marked by the star.

west (SW), and southeast (SE). The length of the cluster-mean trajectories indicates the transport speed of air masses. In this analysis, the long and fast-moving trajectories were disaggregated into groups originating from more distant SE and SW regions during summer and NW and N regions during other seasons. Members of this cluster have extremely long transport patterns, some of them even cross over In-

ner Mongolia and Mongolia (e.g., N and NW). Trajectories belonging to S–SW and E–SE typically followed flow patterns from the South Sea and Pacific Ocean, respectively. Otherwise, some trajectories have short transport patterns, indicative of slow-moving air masses. Most of the pollution episodes within this group are probably enriched from regional and local emission sources. Such trajectories were

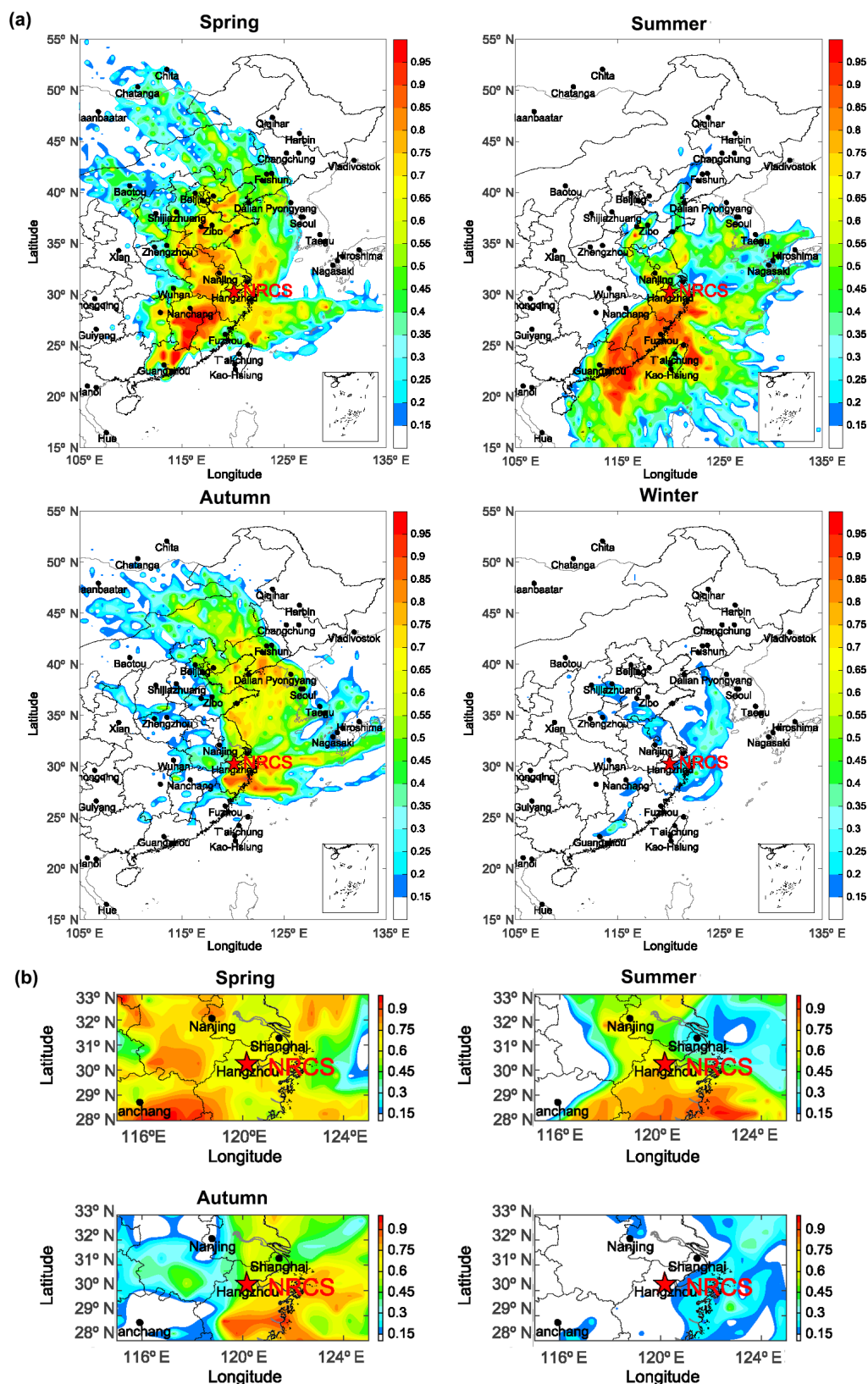
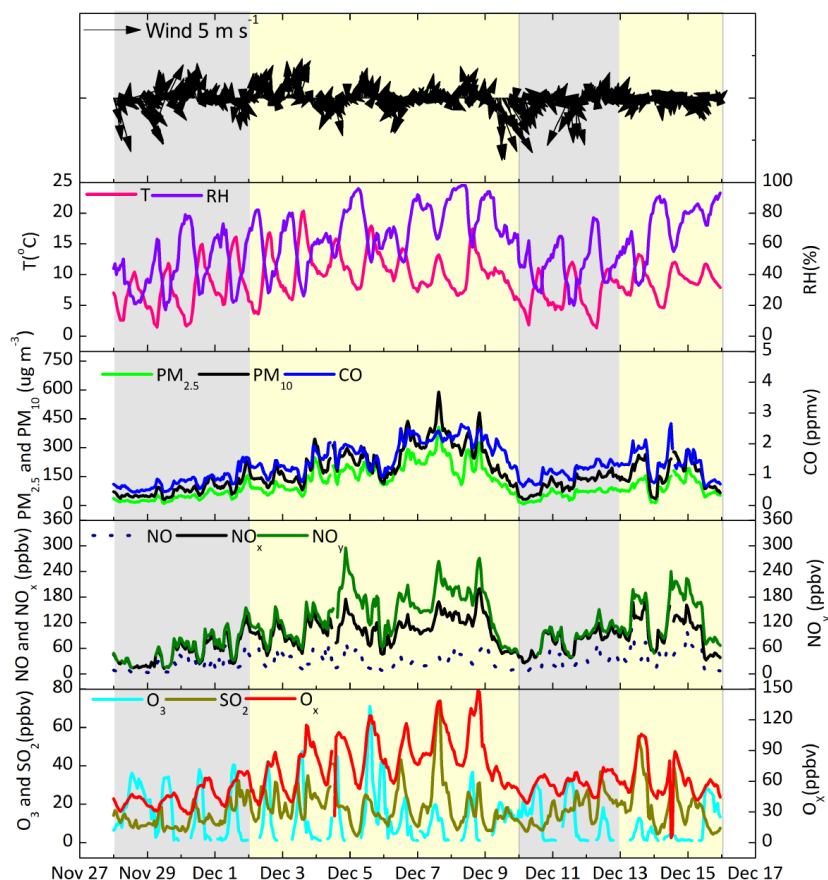


Figure 7. (a) Same as Fig. 6a but for  $O_3$ . (b) The zoomed view of Fig. 7a.



**Figure 8.** Time series of meteorological parameters and chemical species before, during, and after the haze period. The gray shaded area indicates the Phase I (28 November–1 December) and Phase II (10–12 December), and the yellow shaded area represents haze events Phase III (2–9 December) and Phase IV (13–15 December).

also identified during every season in our study. For instance, the air masses associated with cluster 4 (in spring, autumn, and winter) and cluster 1 in summer predominantly originated from local areas and nearby provinces with significant pollution sources, such as Jiangsu, Anhui, and Shanghai.

Table 3 summarizes the percentages of these identified trajectory clusters on a seasonal basis as well as the corresponding mean concentrations of  $\text{PM}_{2.5}$  and other trace gases related to each trajectory cluster. As inferred from Table 3, the clusters exhibited larger variability and season dependence: the predominant clusters were W (42.7 %) in spring, SW (53.9 %) in summer, NW (35.5 %) in autumn, and N (54.9 %) in winter, respectively. It is of interest to note that some trajectory clusters with small percentages are highly related with high pollutants' concentrations. In summer, a few  $\text{PM}_{2.5}$  pollution cases (only 8.4 % of the summertime trajectories) with mean concentration as high as  $51.5 \mu\text{g m}^{-3}$  were related with the N trajectories traveling across the cluster of strongly industrialized cities (i.e., Suzhou, Wuxi, and Changzhou).

Furthermore, we depicted the seasonal WPSCF maps (a), the corresponding zoomed maps (b), and the emissions maps (c) for  $\text{PM}_{2.5}$ ,  $\text{O}_3$ , CO,  $\text{NO}_x$ , and  $\text{SO}_2$ , respectively, denoted with letters a, b, and c in the figure captions. Here we presented the results of two representative species,  $\text{PM}_{2.5}$  (Fig. 6a, b, and c) and  $\text{O}_3$  (Fig. 7a, b), and those of the other species were included in the Supplement (Figs. S3a, S5c). Judging from the WPSCF maps, together with their corresponding zoomed views and the calculated emissions maps, a few distinct features were summarized. (1) Local emissions were significant for the primary pollutants such as CO (Fig. S3),  $\text{NO}_x$  (Fig. S4),  $\text{SO}_2$  (Fig. S5), and  $\text{PM}_{2.5}$  (Fig. 6) on a seasonal scale. For  $\text{O}_3$ , local photochemistry dominated during spring, summer, and autumn (Fig. 7a, b) due to strong photochemical reactivity. (2) The potential sources of CO and  $\text{NO}_x$  had similar patterns on spatial and seasonal scales, with higher values in the NW during spring, covering the mid-YRD regions across Anhui Province and reaching the border of Henan Province, and in the NW and N during autumn and winter, covering most of Jiangsu Province and part of Shandong Province, including the cities of Jinan and Zibo.

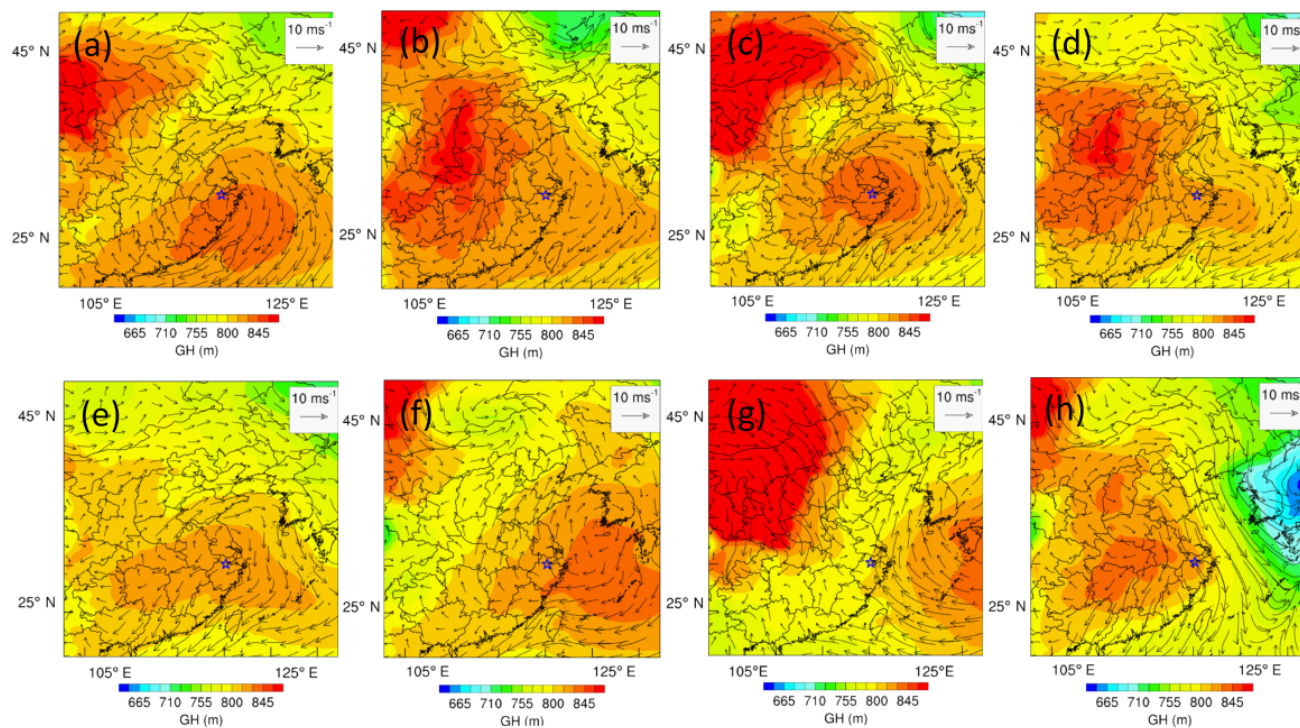


**Figure 9.** The geopotential height field (GH) (indicated by color bars) and wind field (WF) (black vectors) for 925 hPa at 20:00 LT during 2–9 December 2013. All panels represent 2–5 and 6–9 December from left to right on the top and bottom. The NRCS is marked by the star.

(3) Higher values for  $\text{SO}_2$  were located in the city of Ningbo and on the coast of the Yellow Sea during spring, in the southeastern region from the East Sea during summer, probably due to ship emissions (Fan et al., 2016), but in the inland cities such as Shaoxing and Quzhou of Zhejiang Province during autumn and Anhui Province during winter. In total, along with the air mass trajectories, the WPSCF maps for these primary pollutants were generally in line with their respective corresponding species' emissions (Figs. 6c, S3c, S4c, and S5c). Although no seasonal patterns in emission maps were found, the emissions of these pollutants exhibited interspecies similarity and strong spatial dependence with the industrialization level.

In terms of  $\text{PM}_{2.5}$ , the potential sources showed distinct seasonal variations such as southeastern regions of Jiangxi Province and the northwestern area of Zhejiang Province during spring and in the western cities of North Korea (Pyongyang) and South Korea (Seoul) with the northeasterly air mass across the Yellow Sea during summer. As illustrated in Fig. 6a and b, the contributions from local emissions were both found to be more significant for autumn and winter than spring and summer, covering all the cities in Zhejiang Province, especially in the south and southwest (e.g., cities of Lishui, Jinhua, and Quzhou). Moreover, we found higher WPSCF values located in the central cities of Jiangsu Province in autumn and the expanded area towards the whole Jiangsu and Anhui Province and the southeastern

coastal cities (e.g., Wenzhou, Ningbo in Zhejiang Province, Fuzhou in Fujian Province) in winter, revealing that cross-boundary transport is crucial to the pollution of particulate matter. This result has been confirmed by Yu et al. (2014), who also found that such transport dominated in the city of Hangzhou during the heavy haze episode (3–9 December 2013).

For  $\text{O}_3$ , its potential sources should be interpreted with caution since it is not directly emitted to the atmosphere and has complicated chemistry involved with VOCs and  $\text{NO}_x$ . The majority of the measured  $\text{O}_3$  is probably formed by photooxidation in the vicinity of the measurement site (Fig. 7b), specified as the local contribution, but clear differences associated with regional transport are illustrated in Fig. 7a. In spring, high  $\text{O}_3$  concentrations were connected with air masses coming from western and southwestern regions (e.g., Anhui, Jiangxi, and mid-Guangdong Province) and northwestern areas such as Jiangsu, Henan, and Shandong Province; in summer, more extensive potential sources were elucidated to be located in the eastern, southern, and southwestern regions of China, covering the southern part of Zhejiang Province, southeastern cities of Jiangxi Province, almost the whole of Fujian Province, the eastern part of Guangdong Province, and the mid-Zhejiang Province (e.g., cities of Quzhou, Jinhua, and Ningbo). A very interesting finding should be pointed out that air masses that were transported from the offshore areas of the Yellow Sea, East Sea,

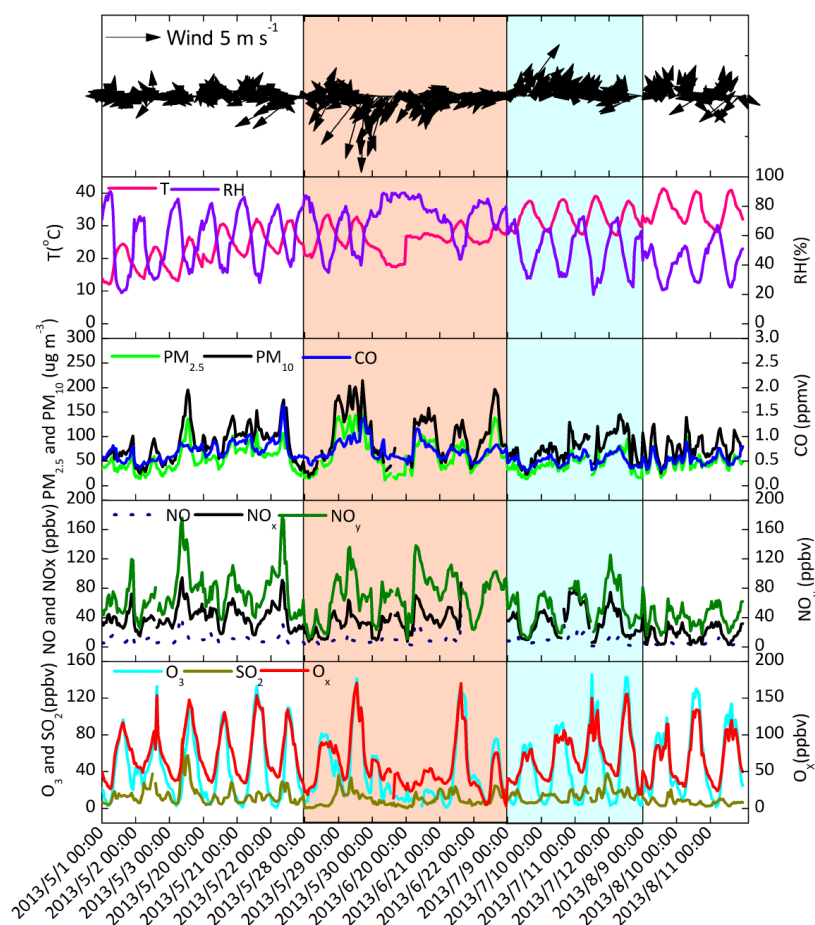


**Figure 10.** Same as Fig. 8 but during the photochemical pollution period. The orange shaded area represents Phase I (28–30 May and 20–22 June), the cyan shaded area indicates Phase II (9–12 July), and the other area represents Phase III (1–3 May, 20–22 May, and 9–11 August).

and South Sea to southeastern Zhejiang, Jiangsu, and Fujian Province, respectively, were also found to be highly relevant to the elevated  $O_3$  at the NRCS site. This was also well evidenced by seasonal and spatial distributions of  $O_3$  volume mixing ratio simulated by MOZART-4/GEOS-5 (see Fig. S6). We speculated that the recirculation of pollutants by sea- and land-breeze circulations around the cities along the YRD and Hangzhou Bay, which has been confirmed by M. M. Li et al. (2015, 2016), was largely responsible for the increased concentration of  $O_3$  at the NRCS site. Such an increase in  $O_3$  concentrations in urbanized coastal areas has been observed and modeled in a number of studies (Oh et al., 2006; Levy et al., 2008; Martins et al., 2012). Thus, our study further emphasizes the importance of local thermally induced circulation for air quality.

### 3.5 Cases studies for haze (high $PM_{2.5}$ ) and photochemical pollution (high $O_3$ ) episodes

To elucidate the specific causes of high  $PM_{2.5}$  and  $O_3$  episodes including the transport and local photochemical for-

mation, we chose two typical cases for detailed interpretations, and these are presented here. In this study, the haze pollution episode is defined as the event that consists of continuous days with daily averaged  $PM_{2.5}$  concentration exceeding  $75 \mu\text{g m}^{-3}$ , which has also been used to distinguish non-haze and haze episode in other studies (Yu et al., 2014; J. Wu et al., 2016). With respect to this campaign, there were two non-haze episodes (Phases I: 28 November–1 December and II: 10–12 December) and their subsequent severe haze pollution episodes (Phases III: 2–9 December and IV: 13–15 December) at the NRCS site, as illustrated in Fig. 8. Phase III showed that high  $PM_{2.5}$  (up to  $406 \mu\text{g m}^{-3}$ ) appeared on 7 December, and broad  $PM_{2.5}$  peaks (around  $300 \mu\text{g m}^{-3}$ ) occurred before and after 2 days. Simultaneously, CO,  $SO_2$ , and  $NO_x$  also reached very high levels on this day, confirming that the common origin of CO and  $PM_{2.5}$  is from heating and combustion and the rapid conversion of  $SO_2$  and  $NO_x$  to sulfate and nitrate in  $PM_{2.5}$  in winter. But for  $O_3$ , its level reached as low as 11.5 ppbv at 15:00 LT on that day, owing to the weak photochemical activity under the severe haze pollution. Along with the high  $NO_2$  concentration

**Table 3.** Mean concentrations of PM<sub>2.5</sub> ( $\mu\text{g m}^{-3}$ ) and other trace gases (units of ppmv for CO but ppbv for other gases) in the identified trajectory clusters within the four-season period, together with the percentages of each trajectory cluster.

Season	Cluster	Percent (%)	PM <sub>2.5</sub>	O <sub>3</sub>	SO <sub>2</sub>	CO	NO <sub>x</sub>
Spring	1	12.1	45.0	28.3	10.7	0.7	38.3
	2	16.6	44.3	31.6	13.2	0.7	39.1
	3	16.0	35.3	30.5	9.7	0.6	34.5
	4	42.6	52.4	23.2	11.4	0.8	42.5
	5	5.5	38.2	34.2	11.2	0.7	37.9
	6	7.2	58.1	34.2	11.9	0.8	43.8
Summer	1	8.4	51.5	24.6	7.9	0.8	29.2
	2	8.6	34.2	35.2	9.2	0.5	22.8
	3	22.6	24.0	28.7	7.9	0.4	21.7
	4	31.3	38.2	36.8	9.1	0.5	24.4
	5	19.4	38.7	27.2	8.9	0.6	28.7
	6	9.7	22.4	26.7	7.5	0.4	17.6
Autumn	1	23.6	42.1	27.4	9.9	0.7	36.9
	2	32.5	50.7	24.6	8.2	0.8	39.4
	3	8.3	21.7	19.8	8.0	0.5	22.0
	4	7.8	68.6	34.8	8.4	0.8	38.8
	5	11.9	49.9	22.6	10.1	0.7	40.8
	6	15.9	79.6	21.6	12.9	0.9	62.0
Winter	1	7.1	60.9	16.6	15.4	1.3	53.7
	2	24.2	83.3	14.4	15.9	1.4	65.4
	3	16.4	47.3	14.0	11.9	1.1	42.7
	4	21.8	75.9	11.9	13.5	1.5	63.1
	5	16.8	67.0	11.7	13.1	1.5	53.7
	6	13.7	102.1	14.4	16.9	1.4	81.0

(around 120 ppbv), it could not produce sufficient conversion oxidants (OH and HO<sub>2</sub> radicals) for the gas-phase oxidation of SO<sub>2</sub> (Poppe et al., 1993; Hua et al., 2008), while the increased relative humidity during 6–8 December possibly favored the aqueous-phase oxidation of SO<sub>2</sub>.

Moreover, according to the results obtained from the backward trajectory cluster and WPSCF analysis during 2–9 December 2013 (Fig. S7), we found an apparent contribution from the transported air mass from northwestern regions such as Jiangsu Province and Anhui Province. Our results were in good agreement with contemporaneous measurement in Hangzhou (J. Wu et al., 2016). Subsequently, at the end of this episode, significant drops of these species except O<sub>3</sub> were observed from 00:00 to 23:00 LT on 9 December (i.e., 189 to 41.6  $\mu\text{g m}^{-3}$  for PM<sub>2.5</sub>, 2.3 to 1.0 ppmv for CO, and 145 to 47.9 ppbv for NO<sub>x</sub>). Weather chart and wind data suggested that the region of NRCS was always controlled by a strong continental high pressure system originating from the northwest before 8 December (Fig. 9a–f) but that this rapidly changed to be dominated under a strong marine high pressure system coming from the east at 02:00 LT on 9 December (Fig. 9g–h), which brought clean maritime air passing over the Yellow Sea and thus caused such decreases in these pollutants. However, it quickly turned back to be controlled under a continental high pressure system described above, carry-

ing pollutants from the city clusters to the NRCS site. This could account for the accumulations of these species during the intermediate period (Phase II). The subsequent Phase IV with high PM<sub>2.5</sub> episode was also found to be governed by a stagnant high pressure over the YRD region (Fig. S8).

For the photochemical pollution events, we selected three cases with O<sub>3</sub> exceedances (74.6 ppbv) during May–August according to Grade II standard of CAAQS. As displayed in Fig. 10, they were Phase I (28–30 May and 20–22 June), with a rapid buildup and decrease of O<sub>3</sub> within 3 days, Phase II (9–12 July), representing a distinct accumulation process of O<sub>3</sub> exceedances, and Phase III (1–3 and 20–22 May, and 9–11 August), with high O<sub>3</sub> levels within three consecutive days. For 28 May in Phase I, the weather chart suggested that a strong anticlockwise cyclone was located over the YRD. In this case, the cyclone (i.e., low pressure) caused favoring conditions for pollution diffusion, e.g., cloudy weather and high wind velocities. Then, a strong clockwise anticyclone from the northwest, sweeping over the cluster of cities (i.e., Nanjing and Shanghai), rapidly moved adjacent to the NRCS site on 29 May. It carried the primary pollutants such as CO, SO<sub>2</sub>, and NO<sub>x</sub> from these megacities, and secondary products (i.e., O<sub>3</sub> and some NO<sub>2</sub>) were further produced via complex photochemical reactions under such synoptic conditions. As the orange shaded area shows in Fig. 10, the hourly maximums of O<sub>3</sub> and PM<sub>2.5</sub> were observed to be as high as 141.2 ppbv and 135.8  $\mu\text{g m}^{-3}$  at 13:00 LT on 29 May. Following this day, the cyclone dominated this region again and caused a sudden decrease in atmospheric pollutants. Also, a similar case was found during 20–22 June under such changes in synoptic weather. For Phase II (9–12 July), a typical accumulation process was observed, with the daily maximums of atmospheric pollutants increasing from 90.4 to 142.9 ppbv for O<sub>3</sub>, 77.6 to 95.3  $\mu\text{g m}^{-3}$  for PM<sub>2.5</sub>, and 80.2 to 125.2 ppbv for NO<sub>y</sub>. The examination of the day-to-day 925 hPa synoptic chart derived from NCEP reanalysis suggested that a high pressure system governed over the YRD during 9–11 July, with southwesterly prevailing wind. The air masses recorded at this site mainly came from the most polluted city clusters in the southwest (e.g. Zhejiang, Jiangxi, and Fujian Province). Meanwhile, the stagnant synoptic condition (i.e., low wind speed) favored the accumulation of primary pollutants such as CO and NO<sub>x</sub>. Secondary pollutants O<sub>3</sub> and PM<sub>2.5</sub> were also rapidly formed via photochemical oxidation, and they further accumulated under such synoptic conditions, together with continuous high temperature (daily mean around 33 °C). On 12 July, a typhoon named Soulik moved to a location a few hundred kilometers away from the NRCS site, bringing southeasterly maritime air over the YRD. Daily maximum O<sub>3</sub> reached 142.8 ppbv at 12:00 LT, even with a low concentration of precursors (i.e., 0.48 ppmv for CO and 16.0 ppbv for NO<sub>x</sub>), suggesting high photochemical production efficiency of O<sub>3</sub> in this region in summer. This phenomenon has also been found in the multi-day episode of high O<sub>3</sub> in Nanjing during 20–21 July 2011

(Ding et al., 2013). In this phase, PM<sub>2.5</sub> mass concentration showed very good correlation ( $R = 0.79$ ,  $p < 0.001$ ) with O<sub>3</sub> during the daytime (09:00–17:00 LT), possibly indicating a common origin of BVOCs due to the significant vegetation emission as discussed above, in addition to high biomass production in the southern part of the YRD (Ding et al., 2013). For Phase III (1–3 and 20–22 May, and 9–11 August), there were mostly sunny days with low wind speed and moderate/high air temperature, which were both beneficial factors for the photochemical formation of O<sub>3</sub>, together with sufficient precursors (NO<sub>x</sub> and VOCs) in the summer and early autumn over YRD. For 1–3 and 20–22 May, daily maximum  $T$  values were moderate (around 25 °C versus 31 °C), while the daily maximums of NO<sub>x</sub> reached as high as 43–95 and 50–90 ppbv, with both favoring the photochemical formation to produce the continuous high O<sub>3</sub> concentrations (daily maximums: 96–133 ppbv via 104–133 ppbv). The reverse case is also true during 9–11 August, on which the daily maximum  $T$  and NO<sub>x</sub> ranged 40.6–41.4 °C and 33–44 ppbv, respectively, resulting in the production of continuously high O<sub>3</sub> from 98.8 to 130.5 ppbv.

### 3.6 Photochemical age and ozone production efficiency during photochemical pollution and haze period

Photochemical age is often used to express the extent of photochemistry, which can be estimated using an indicator such as NO<sub>x</sub>/NO<sub>y</sub> (Carpenter et al., 2000; Lin et al., 2008, 2009, 2011; Parrish et al., 1992). Air masses with fresh emissions have an NO<sub>x</sub>/NO<sub>y</sub> ratio close to 1, while there is a lower NO<sub>x</sub>/NO<sub>y</sub> ratio for the photochemical aged air masses. In this study, for the haze events mentioned above, the average and maximum NO<sub>x</sub>/NO<sub>y</sub> ratios were as high as 0.80 and 0.99, respectively, indicating that photochemical conversion of NO<sub>x</sub> is not absent but fairly slow. This was quite consistent with the largely weakened photochemistry due to the low intensity of UV radiation in winter. In contrast, during the photochemical pollution period, they were as low as 0.53 and 0.14 for the average and minimum ratio. The simultaneous measurements of atmospheric O<sub>3</sub>, NO<sub>x</sub>, and NO<sub>y</sub> can provide an insight into calculating the ozone production efficiency (OPE) for different seasons. From the data of O<sub>x</sub> and NO<sub>z</sub>, the ratio of  $\Delta(O_x) / \Delta(NO_z)$  can be calculated as a kind of observation-based OPE (Trainer et al., 1993; Sillman, 2000; Kleinman et al., 2002; Lin et al., 2011). In this study, the mean values of NO<sub>z</sub> and O<sub>x</sub> between 07:00 and 15:00 LT were used to calculate the OPE values through linear regression. In addition, these data were also confined to sunny days and wind speeds below 3 m s<sup>-1</sup>, reflecting the local photochemistry as possible. The OPE value during the photochemical pollution period (SOPE) mentioned above was 1.99, generally within the reported range of 1–5 in the PRD cities, but lower than 3.9–9.7 in the summer in Beijing (Chou et al., 2009; Ge et al., 2012). Meanwhile, the OPE value of 0.77 during the haze period (HOPE) was

also comparable with the reported value of 1.1 in winter in Beijing (Lin et al., 2011). The smaller winter OPE value in Hangzhou might be ascribed to the weaker photochemistry and higher NO<sub>x</sub> concentration. At a high NO<sub>x</sub> level, OPE tends to decrease with the increased NO<sub>x</sub> concentration (Ge et al., 2010; Lin et al., 2011). In Hangzhou, the NO<sub>x</sub> level is frequently higher than needed for producing photochemical O<sub>3</sub>, and excessive NO<sub>x</sub> causes net O<sub>3</sub> loss rather than accumulation. In this study, 75 % of daily OPE values were negative, which can be explained by two factors. To some extent, due to the geographical location and unique climate characteristics of Hangzhou as depicted above, the interference of non-beneficial meteorological conditions existed in the formation of local O<sub>3</sub> deriving from photochemistry, i.e., strong wind, frequent rainy days. The other factor points to the consumption of O<sub>3</sub> by excessive NO<sub>x</sub>, which was also confirmed by the conclusion that Hangzhou was mostly in the VOC-limited regime as discussed in Sect. 3.2. Such a circumstance was also observed at the rural site of Gucheng in the North China Plain (NCP) and in the urban area of Beijing (Lin et al., 2009, 2011). Taking the average of SOPE of 1.99 and the average daytime increment of NO<sub>z</sub> (ca. 20 ppbv), we estimated an average photochemical O<sub>3</sub> production of about 39.8 ppbv during the photochemical pollution period. In contrast, the lower average photochemical O<sub>3</sub> production was estimated to be 10.78 ppbv during the haze period based on HOPE, which might act as a significant source of surface O<sub>3</sub> in winter in Hangzhou.

## 4 Conclusions

In this study, we presented an overview of 1-year measurements of trace gases (O<sub>3</sub>, CO, NO<sub>x</sub>, NO<sub>y</sub>, and SO<sub>2</sub>) and particulate matter (PM<sub>2.5</sub> and PM<sub>10</sub>) at the National Reference Climatological Station in Hangzhou. The characteristics and causes of these chemicals were investigated through examination of their seasonal characteristics, along with comparison with previous results in other regions in China, interspecies correlations, and the concentration dependence on local emission and regional transport. Specific photochemical pollution and haze cases were studied in detail based on discussion of the physical processes and photochemical formation (ozone production efficiency). The main findings and conclusions are summarized below.

- Within a 1-year study period, there were 38 days of O<sub>3</sub> exceedances and 62 days of PM<sub>2.5</sub> exceedances of the National Ambient Air Quality Standards in China at the site, suggesting heavy air pollution in this region. In general, the concentration levels of these chemicals were consistent with those observed by other contemporaneous measurements in Hangzhou and the other cities in the YRD, but lower than those in the NCP. Distinct seasonal characteristics were found with a broad peak in late spring and middle summer and a minimum in win-

ter for O<sub>3</sub>, while there was a maximum in winter and a minimum in summer for PM<sub>2.5</sub>.

- b. A positive O<sub>3</sub>–NO<sub>y</sub> correlation was found for air masses with high air temperature in summer, suggesting a strong local photochemical production of O<sub>3</sub>. In addition, correlation analysis shows an important conversion of SO<sub>2</sub> to sulfate and NO<sub>x</sub> to nitrate and/or deposition in humid conditions. CO–NO<sub>y</sub>–O<sub>3</sub> correlation suggested a VOC-limited regime for the overall study period, but this moved toward an optimum O<sub>3</sub> production zone during warm seasons. The positive correlation between O<sub>3</sub> and PM<sub>2.5</sub> under high air temperature indicated a formation of secondary fine particulates in warm seasons.
- c. The results from the emission inventories of the primary pollutants such as PM<sub>2.5</sub>, CO, NO<sub>x</sub>, and SO<sub>2</sub> demonstrated that local emissions were both significant for these species but without distinct seasonal variations. The major potential sources of PM<sub>2.5</sub> were located in the southwestern regions in spring, northwestern and northeastern regions in summer, and northwestern regions (the whole Jiangsu Province and Anhui Province) in autumn and winter. CO and NO<sub>x</sub> showed similar patterns to northwestern regions covering the mid-YRD regions and Anhui Province during spring and in the northwestern and northern regions, including Jiangsu Province and part of Shandong Province, during autumn and winter. The distinct seasonal variation in SO<sub>2</sub> potential might be from southwestern and eastern regions during spring and summer but northwestern regions during autumn and winter. Air masses transported from the offshore areas of the Yellow Sea, East Sea, and South Sea to southeastern Zhejiang, Jiangsu, and Fujian Province, respectively, were also found to be highly relevant to the elevated O<sub>3</sub> at the NRCS site, probably due to the recirculation of pollutants by sea- and land-breeze circulations around the cities along the YRD and Hangzhou Bay. This finding further emphasizes the importance of urban-induced circulation for air quality.
- d. Case studies for photochemical pollution and haze episodes both suggest the combined importance of local atmospheric photochemistry and synoptic weather during the accumulation (related with anticyclones) and dilution process (related with cyclones) of these episodes. The average photochemical O<sub>3</sub> production was estimated to be 39.8 and 10.78 ppbv during photochemical pollution and haze periods, respectively, indicating that local photochemistry might act as a significant source of surface O<sub>3</sub> in winter in Hangzhou.

Our study further completes a picture of air pollution in the YRD, interprets the physical and photochemical processes during haze and photochemical pollution episodes, and explores the seasonal and spatial variations in the potential

sources of these pollutants. Moreover, this work suggests that the cross-region control measures are crucial to improve air quality in the YRD region, and it further emphasizes the importance of local thermally induced circulation for air quality.

*Data availability.* The data in the figures in both the main text and the Supplement are available upon request to the corresponding author (Gen Zhang, zhanggen@cma.gov.cn).

**The Supplement related to this article is available online at <https://doi.org/10.5194/acp-18-1705-2018-supplement>.**

*Competing interests.* The authors declare that they have no conflict of interest.

*Acknowledgements.* This study is financially supported by the National Key Research and Development Program of China (2016YFC0202300), the National Natural Science Foundation of China (41775127 and 41505108), and the Shanghai Key Laboratory of Meteorology and Health (QXJK201501). The authors are especially grateful to Miao Yucong for the technical support in drawing some of the figures and giving some valuable comments in the discussions.

Edited by: Rolf Müller

Reviewed by: two anonymous referees

## References

- Atkinson, R.: Atmospheric chemistry of VOCs and NO<sub>x</sub>, *Atmos. Environ.*, 34, 2063–2101, 2000.
- Böge, O., Mutzel, A., Linuma, Y., Yli-Pirilä, P., Kahnt, A., Joutsensaari, J., and Herrmann, H.: Gas-phase products and secondary organic aerosol formation from the ozonolysis and photooxidation of myrcene, *Atmos. Environ.*, 79, 553–560, 2013.
- Calfapietra, C., Fares, S., Manes, F., Morani, A., Sgrign, G., and Loreto, F.: Role of biogenic volatile organic compounds (BVOC) emitted by urban trees on ozone concentration in cities: A review, *Environ. Pollut.*, 183, 71–80, 2013.
- Cao, J., Shen, Z., Chow, J. C., Qi, G., and Watson, J. G.: Seasonal variations and sources of mass and chemical composition for PM<sub>10</sub> aerosol in Hangzhou, China, *Particuology*, 7, 161–168, 2009.
- Carpenter, L. J., Green, T. J., Mills, G. P., Bauguette, S., Penkett, S. A., Zanis, P., Schuepbach, E., Schmidbauer, N., Monks, P. S., and Zellweger, C.: Oxidized nitrogen and ozone production efficiencies in the springtime free troposphere over the Alps, *J. Geophys. Res.*, 105, 14547–14559, 2000.
- Chai, F. H., Gao, J., Chen, Z. X., Wang, S. L., Zhang, Y. C., Zhang, J. Q., Zhang, H. F., Yun, Y. R., and Ren, C.: Spatial and temporal

- variation of particulate matter and gaseous pollutants in 26 cities in China, *J. Environ. Sci.*, 26, 75–82, 2014.
- Chang, J., Ren, Y., Shi, Y., Zhu, Y. M., Ge, Y., Hong, S. M., Jiao, L., Lin, F. M., Peng, C. H., Mochizuki, T., Tani, A., Mu, Y., and Fu, C. X.: An inventory of biogenic volatile organic compounds for a subtropical urban-rural complex, *Atmos. Environ.*, 56, 115–123, 2012.
- Chen, T., He, J., Lu, X., She, J., and Guan, Z.: Spatial and temporal variations of PM<sub>2.5</sub> and its relation to meteorological factors in the urban area of Nanjing, China, *Int. J. Env. Res. Pub. He.*, 13, 921, <https://doi.org/10.3390/ijerph13090921>, 2016.
- Cheng, Y. F., Zheng, G. J., Wei, C., Mu, Q., Zheng, B., Wang, Z. B., Gao, M., Zhang, Q., He, K. B., Carmichael, G., Pöschl, U., and Su, H.: Reactive nitrogen chemistry in aerosol water as a source of sulfate during haze events in China, *Science Advances*, 2, 1–11, 2016.
- Chou, C. K., Tsai, C. Y., Shiu, C. J., Liu, S. C., and Zhu, T.: Measurement of NO<sub>y</sub> during campaign of air quality research in Beijing 2006 (CAREBeijing-2006): implications for the ozone production efficiency of NO<sub>x</sub>, *J. Geophys. Res.*, 114, 328–334, 2009.
- Chow, J. C. and Watson, J. G.: Review of PM<sub>2.5</sub> and PM<sub>10</sub> apportionment for fossil fuel combustion and other sources by the chemical mass balance receptor model, *Energy Fuels*, 16, 222–260, 2002.
- Claeys, M., Graham, B., Vas, G., Wang, W., Vermeylen, R., Pashynska, V., Cafmeyer, J., Guyon, P., Andreae, M. O., Artaxo, P., and Maenhaut, W.: Formation of secondary organic aerosols through photooxidation of isoprene, *Science*, 303, 1173–1176, 2004.
- Dickerson, R. R., Kondragunta, S., Stenichkov, G., Civerolo, K. L., Doddridge, B. G., and Holben, B. N.: The Impact of aerosols on solar ultraviolet radiation and photochemical pollution, *Science*, 278, 827–830, 1997.
- Ding, A. J., Wang, T., Thouret, V., Cammas, J.-P., and Nédélec, P.: Tropospheric ozone climatology over Beijing: analysis of aircraft data from the MOZAIC program, *Atmos. Chem. Phys.*, 8, 1–13, <https://doi.org/10.5194/acp-8-1-2008>, 2008.
- Ding, A. J., Fu, C. B., Yang, X. Q., Sun, J. N., Zheng, L. F., Xie, Y. N., Herrmann, E., Nie, W., Petäjä, T., Kerminen, V.-M., and Kulmala, M.: Ozone and fine particle in the western Yangtze River Delta: an overview of 1 yr data at the SORPES station, *Atmos. Chem. Phys.*, 13, 5813–5830, <https://doi.org/10.5194/acp-13-5813-2013>, 2013.
- Fan, Q., Zhang, Y., Ma, W., Ma, H., Feng, J., Yu, Q., Yang, X., Ng, S. K. W., Fu, Q., and Chen, L.: Spatial and seasonal dynamics of ship emissions over the Yangtze River Delta and East China Sea and their potential environmental influence, *Environ. Sci. Technol.*, 50, 1322–1329, 2016.
- Feng, Z. Z., Sun, J. S., Wan, W. X., Hu, E. Z., and Calatayud, V.: Evidence of widespread ozone-induced visible injury on plants in Beijing, China, *Environ. Pollut.*, 193, 296–301, 2014.
- Ge, B. Z., Xu, X. B., Lin, W. L., and Wang, Y.: Observational study of ozone production efficiency at the Shangdianzi regional background station, *Environm. Sci.*, 31, 1444–1450, 2010 (in Chinese with English abstract).
- Ge, B. Z., Xu, X. B., Lin, W. L., Li, J., and Wang, Z. F.: Impact of the regional transport of urban Beijing pollutants on downwind areas in summer: ozone production efficiency analysis, *Tellus B*, 64, 17348, <https://doi.org/10.3402/tellusb.v64i0.17348>, 2012.
- Geng, F. H., Zhao, C. S., Tang, X., Lu, G. L., and Tie, X. X.: Analysis of ozone and VOCs measured in Shanghai: A case study, *Atmos. Environ.*, 41, 989–1001, 2007.
- Guenther, A., Hewitt, C. N., Erickson, D., Fall, R., Geron, C., Graedel, T., Harley, P., Klinger, L., Lerdau, M., McKay, W. A., Pierce, T., Scholes, B., Steinbrecher, R., Tallamraju, R., Taylor, J., and Zimmerman, P. L.: A global model of natural volatile organic compound emissions, *J. Geophys. Res.*, 100, 8873–8892, 1995.
- Guo, H., Wang, T., Simpson, I. J., Blake, D. R., Yu, X. M., Kwok, Y. H., and Li, Y. S.: Source contributions to ambient VOCs and CO at a rural site in eastern China, *Atmos. Environ.*, 38, 4551–4560, 2004.
- He, K. B., Huo, H., and Zhang, Q.: Urban air pollution in China: current status, characteristics, and progress, *Annu. Rev. Energ. Env.*, 27, 397–431, 2002.
- Hsu, Y. K., Holsen, T. M., and Hopke, P. K.: Comparison of hybrid receptor models to locate PCB sources in Chicago, *Atmos. Environ.*, 37, 545–562, 2003.
- Hua, W., Chen, Z. M., Jie, C. Y., Kondo, Y., Hofzumahaus, A., Takegawa, N., Chang, C. C., Lu, K. D., Miyazaki, Y., Kita, K., Wang, H. L., Zhang, Y. H., and Hu, M.: Atmospheric hydrogen peroxide and organic hydroperoxides during PRIDE-PRD'06, China: their concentration, formation mechanism and contribution to secondary aerosols, *Atmos. Chem. Phys.*, 8, 6755–6773, <https://doi.org/10.5194/acp-8-6755-2008>, 2008.
- Huang, Y., Shen, H. Z., Chen, H., Wang, R., Zhang, Y. Y., Su, S., Chen, Y. C., Lin, N., Zhao, S. J., Zhong, Q. R., Wang, X. L., Liu, J. F., Li, B. G., Liu, W. X., and Tao, S.: Quantification of global primary emissions of PM<sub>2.5</sub>, PM<sub>10</sub>, and TSP from combustion and industrial process sources, *Environ. Sci. Technol.*, 48, 13834–13843, 2014.
- IPCC: Summary for Policymakers, in: *Climate Change 2007: The Physical Science Basis. Contribution of Working Group I to the Fourth Assessment Report of the Intergovernmental Panel on Climate Change*, edited by: Solomon, S., Qin, D., Manning, M., Chen, Z., Marquis, M., Averyt, K. B., Tignor, M., and Miller, H. L., Cambridge University Press, Cambridge, United Kingdom and New York, NY, USA, 2007.
- Jansen, R. C., Shi, Y., Chen, J. M., Hu, Y. J., Xu, C., Hong, S. M., Jiao, L., and Zhang, M.: Using hourly measurements to explore the role of secondary inorganic aerosol in PM<sub>2.5</sub> during haze and fog in Hangzhou, China, *Adv. Atmos. Sci.*, 31, 1427–1434, 2014.
- Kamens, R., Jang, M., Chien, C. J., and Leach, K.: Aerosol formation from reaction of  $\alpha$ -pinene and ozone using a gas-phase kinetics-aerosol partitioning model, *Environ. Sci. Technol.*, 33, 1430–1438, 1999.
- Kang, H., Zhu, B., Su, J., Wang, H., Zhang, Q., and Wang, F.: Analysis of a long-lasting haze episode in Nanjing, China, *Atmos. Res.*, 120–121, 78–87, 2013.
- Khoder, M. I.: Atmospheric conversion of sulfur dioxide to particulate sulfate and nitrogen dioxide to particulate nitrate and gaseous nitric acid in an urban area, *Chemosphere*, 49, 675–684, 2002.
- Kleinman, L., Daum, P. H., Lee, Y.-N., Nunnermacker, L. J., Springston, S. R., Weinstein-Lloyd, J., and Rudolph, J.: Ozone production efficiency in an urban area, *J. Geophys. Res.*, 107, 4733, <https://doi.org/10.1029/2002JD002529>, 2002.
- Lambe, A. T., Chhabra, P. S., Onasch, T. B., Brune, W. H., Hunter, J. F., Kroll, J. H., Cummings, M. J., Brogan, J. F., Parmar, Y.,

- Worsnop, D. R., Kolb, C. E., and Davidovits, P.: Effect of oxidant concentration, exposure time, and seed particles on secondary organic aerosol chemical composition and yield, *Atmos. Chem. Phys.*, 15, 3063–3075, <https://doi.org/10.5194/acp-15-3063-2015>, 2015.
- Levy, I., Dayan, U., and Mahrer, Y.: A five-year study of coastal recirculation and its effect on air pollutants over the east Mediterranean region, *J. Geophys. Res.*, 113, D16121, <https://doi.org/10.1029/2007JD009529>, 2008.
- Li, K. W., Chen, L. H., Ying, F., White, S. J., Jang, C., Wu, X. C., Gao, X., Hong, S. M., Shen, J. D., Azzi, M., and Cen, K. F.: Meteorological and chemical impacts on ozone formation: A case study in Hangzhou, China, *Atmos. Environ.*, 196, 40–52, <https://doi.org/10.1016/j.atmosres.2017.06.003>, 2017.
- Li, L., An, J. Y., Shi, Y. Y., Zhou, M., Yan, R. S., Huang, C., Wang, H. L., Lou, S. R., Wang, Q., Lu, Q., and Wu, J.: Source apportionment of surface ozone in the Yangtze River Delta, China in the summer of 2013, *Atmos. Environ.*, 144, 194–207, 2016.
- Li, M. M., Mao, Z. C., Song, Y., Liu, M. X., and Huang, X.: Impact of the decadal urbanization on thermally induced circulations in eastern China, *J. Appl. Meteorol. Clim.*, 54, 259–282, 2015.
- Li, M. M., Song, Y., Mao, Z. C., Liu, M. X., and Huang, X.: Impact of thermal circulations induced by urbanization on ozone formation in the Pearl River Delta, China, *Atmos. Environ.*, 127, 382–392, 2016.
- Lin, W., Xu, X., Zhang, X., and Tang, J.: Contributions of pollutants from North China Plain to surface ozone at the Shangdianzi GAW Station, *Atmos. Chem. Phys.*, 8, 5889–5898, <https://doi.org/10.5194/acp-8-5889-2008>, 2008.
- Lin, W. L., Xu, X. B., Ge, B. Z., and Zhang, X. C.: Characteristics of gaseous pollutants at Gucheng, a rural site southwest of Beijing, *J. Geophys. Res.*, 114, 4723–4734, 2009.
- Lin, W. L., Xu, X. B., Ge, B. Z., and Liu, X.: Gaseous pollutants in Beijing urban area during the heating period 2007–2008: variability, sources, meteorological, and chemical impacts, *Atmos. Chem. Phys.*, 11, 8157–8170, 2011.
- Liu, G., Li, J. H., Wu, D., and Xu, H.: Chemical composition and source apportionment of the ambient PM<sub>2.5</sub> in Hangzhou, China, *Particuology*, 18, 135–143, 2015.
- Liu, T., Li, T. T., Zhang, Y. H., Xu, Y. J., Lao, X. Q., Rutherford, S., Chu, C., and Luo, Y.: The short-term effect of ambient ozone on mortality is modified by temperature in Guangzhou, China, *Atmos. Environ.*, 76, 59–67, 2013.
- Logan, J. A.: Tropospheric ozone: Seasonal behavior, trends, and anthropogenic influence, *J. Geophys. Res.*, 90, 10463–10482, 1985.
- Luo, C., St. John, J. C., Zhou, X. J., Lam, K. S., Wang, T., and Chameides, W. L.: A nonurban ozone air pollution episode over eastern China: observations and model simulations, *J. Geophys. Res.*, 105, 1889–1908, 2000.
- Ma, Z. W., Hu, X. F., Sayer, A. M., Levy, R., Zhang, Q., Xue, Y. G., Tong, S. L., Bi, J., Huang, L., and Liu, Y.: Satellite-based spatiotemporal trends in PM<sub>2.5</sub> concentrations: China, 2004–2013, *Environ. Health Persp.*, 124, 184–192, 2016.
- Martins, D. K., Stauffer, R. M., Thompson, A. M., Knepp, T. N., and Pippin, M.: Surface ozone at a coastal suburban site in 2009 and 2010: relationships to chemical and meteorological processes, *J. Geophys. Res.*, 117, D05306, <https://doi.org/10.1029/2011JD016828>, 2012.
- Meagher, J. F., Stockburger, L., Bailey, E. M., and Huff, O.: The oxidation of sulfur dioxide to sulfate aerosols in the plume of a coal-fired power plant, *Atmos. Environ.*, 12, 2197–2203, 1978.
- Mercado, L. M., Bellouin, N., Sitch, S., Boucher, O., Huntingford, C., Wild, M., and Cox, P. M.: Impact of changes in diffuse radiation on the global land carbon sink, *Nature*, 458, 1014–1017, 2009.
- Miao, Y. C., Liu, S. H., Zheng, Y. J., Wang, S., Liu, Z. X., and Zhang, B. H.: Numerical study of the effects of planetary boundary layer structure on the pollutant dispersion within built-up areas, *J. Environ. Sci.*, 32, 168–179, 2015a.
- Miao, Y. C., Hu, X. M., Liu, S. H., Qian, T., Xue, M., Zheng, Y., and Wang, S.: Seasonal variation of local atmospheric circulations and boundary layer structure in the Beijing-Tianjin-Hebei region and implications for air quality, *J. Adv. Model. Earth Syst.*, 7, 1602–1626, <https://doi.org/10.1002/2015MS000522>, 2015b.
- Miao, Y. C., Guo, J. P., Liu, S. H., Liu, H., Zhang, G., Yan, Y., and He, J.: Relay transport of aerosols to Beijing-Tian-Hebei region by multi-scale atmospheric circulations, *Atmos. Environ.*, 165, 35–45, 2017a.
- Miao, Y., Guo, J., Liu, S., Liu, H., Li, Z., Zhang, W., and Zhai, P.: Classification of summertime synoptic patterns in Beijing and their associations with boundary layer structure affecting aerosol pollution, *Atmos. Chem. Phys.*, 17, 3097–3110, <https://doi.org/10.5194/acp-17-3097-2017>, 2017b.
- Ministry of Environmental Protection of China (MEP): Ambient air quality standards (GB 3095–2012), China Environmental Science Press, Beijing, 12 pp., 2012 (in Chinese).
- Oh, I. B., Kim, Y. K., Lee, H. W., and Kim, C. H.: An observational and numerical study of the effects of the late sea breeze on ozone distributions in the Busan metropolitan area, Korea, *Atmos. Environ.*, 40, 1284–1298, 2006.
- Palm, B. B., Campuzano-Jost, P., Day, D. A., Ortega, A. M., Fry, J. L., Brown, S. S., Zarzana, K. J., Dube, W., Wagner, N. L., Draper, D. C., Kaser, L., Jud, W., Karl, T., Hansel, A., Gutiérrez-Montes, C., and Jimenez, J. L.: Secondary organic aerosol formation from in situ OH, O<sub>3</sub>, and NO<sub>3</sub> oxidation of ambient forest air in an oxidation flow reactor, *Atmos. Chem. Phys.*, 17, 5331–5354, <https://doi.org/10.5194/acp-17-5331-2017>, 2017.
- Parrish, D. D., Hahn, C. J., Williams, E. J., Borton, R. B., Fehsenfeld, F. C., Singh, H. B., Shetter, J. D., Gandrud, B. W., and Ridley, B. A.: Indications of photochemical histories of Pacific air masses from measurements of atmospheric trace species at Point Arena, California, *J. Geophys. Res.*, 97, 15883–15901, 1992.
- Polissar, A. V., Hopke, P. K., Paatero, P., Kaufmann, Y. J., Hall, D. K., Bodhaine, B. A., Dutton, E. G., and Harris, J. M.: The aerosol at Barrow, Alaska: long-term trends and source locations, *Atmos. Environ.*, 33, 2441–2458, 1999.
- Pope, C. and Dockery, D.: Epidemiology of particulate effects, in: Air pollution and health, edited by: Holgate, S. T., Koren, H. S., Samet, J. M., and Maynard, R. L., Academic Press, San Diego, 673–705, 1999.
- Poppe, D., Wallasch, M., and Zimmermann, J.: The dependence of the concentration of OH on its precursors under moderately polluted conditions: a model study, *J. Atmos. Chem.*, 16, 61–78, 1993.
- Qi, B., Du, R., Yu, Z., Zhou, B., and Yuan, X.: Characteristics of atmospheric fine particulates concentrations in Hangzhou region, *Environ. Chem.*, 34, 77–82, 2015.

- Qi, H. X., Lin, W. L., Xu, X. B., Yu, X. M., and Ma, Q. L.: Significant downward trend of SO<sub>2</sub> observed from 2005 to 2010 at a background station in the Yangtze Delta region, China, *Science China Chemistry*, 55, 1451–1458, 2012.
- Ravishankara, A. R.: Heterogeneous and multiphase chemistry in the troposphere, *Science*, 276, 1058–1065, 1997.
- Roelofs, G. J. and Lelieveld, J.: Model study of the influence of cross-tropopause O<sub>3</sub> transports on tropospheric O<sub>3</sub> levels, *Tellus B*, 49, 38–55, 1997.
- Saxena, P. and Seigneur, C.: On the oxidation of SO<sub>2</sub> to sulfate in atmospheric aerosols, *Atmos. Environ.*, 21, 807–812, 1987.
- Seinfeld, J. H. and Pandis, S. N.: *Atmospheric Chemistry and Physics: From Air Pollution to Climate Change*, 2nd Edn., John Wiley & Sons, New York, USA, 57–58 and 381–383, 2006.
- Seinfeld, J. H., Carmichael, G. R., Arimoto, R., Conant, W. C., Brechtel, F. J., Bates, T. S., Cahill, T. A., Clarke, A. D., Doherty, S. J., Flatau, P. J., Huebert, B. J., Kim, J., Markowicz, K. M., Quinn, P. K., Russell, L. M., Russell, P. B., Shimizu, A., Shinzuka, Y., Song, C. H., Tang, Y. H., Uno, I., Vogelmann, A. M., Weber, R. J., Woo, J. H., and Zhang, X. Y.: ACE-ASIA – Regional climatic and atmospheric chemical effects of Asian dust and pollution, *B. Am. Meteorol. Soc.*, 85, 367–380, 2004.
- Seltenrich, N.: A clearer picture of China's air using satellite data and ground monitoring to estimate PM<sub>2.5</sub> over time, *Environ. Health Persp.*, 124, A38, <https://doi.org/10.1289/ehp.124-A38>, 2016.
- Shao, M., Tang, X. Y., Zhang, Y. H., and Li, W. J.: City clusters in China: air and surface water pollution, *Front. Ecol. Environ.*, 4, 353–361, 2006.
- Sillman, S.: Ozone production efficiency and loss of NO<sub>x</sub> in power plant plumes: photochemical model and interpretation of measurements in Tennessee, *J. Geophys. Res.*, 105, 9189–9202, 2000.
- Streets, D. G., Fu, J. S., Jang, C. J., Hao, J. M., He, K. B., Tang, X. Y., Zhang, Y. H., Wang, Z. F., and Li, Z. P.: Air quality during the 2008 Beijing Olympic Games, *Atmos. Environ.*, 41, 480–492, 2007.
- Su, S., Li, B. G., Cui, S. Y., and Tao, S.: Sulfur dioxide emissions from combustion in China: from 1990 to 2007, *Environ. Sci. Technol.*, 45, 8403–8410, 2011.
- Sun, G., Yao, L., Jiao, L., Shi, Y., Zhang, Q., Tao, M., Shan, G., and He, Y.: Characterizing PM<sub>2.5</sub> pollution of a subtropical metropolitan area in China, *Atmospheric and Climate Sciences*, 3, 27580, <https://doi.org/10.4236/acs.2013.31012>, 2013.
- Sun, L., Xue, L., Wang, T., Gao, J., Ding, A., Cooper, O. R., Lin, M., Xu, P., Wang, Z., Wang, X., Wen, L., Zhu, Y., Chen, T., Yang, L., Wang, Y., Chen, J., and Wang, W.: Significant increase of summertime ozone at Mount Tai in Central Eastern China, *Atmos. Chem. Phys.*, 16, 10637–10650, <https://doi.org/10.5194/acp-16-10637-2016>, 2016.
- Trainer, M., Parrish, D. D., Buhr, M. P., Norton, R. B., Fehsenfeld, F. C., Anlauf, K. G., Bottenheim, J. W., Tang, Y. Z., Wiebe, H. A., Roberts, J. M., Tanner, R. L., Newman, L., Bowersox, V. C., Meagher, J. F., Olszyna, K. J., Rodgers, M. O., Wang, T., Berresheim, H., Demerjian, K. L., and Roychowdhury, U. K.: Correlation of O<sub>3</sub> with NO<sub>y</sub> in photochemically aged air, *J. Geophys. Res.*, 98, 2917–2925, 1993.
- Wang, R., Tao, S., Ciais, P., Shen, H. Z., Huang, Y., Chen, H., Shen, G. F., Wang, B., Li, W., Zhang, Y. Y., Lu, Y., Zhu, D., Chen, Y. C., Liu, X. P., Wang, W. T., Wang, X. L., Liu, W. X., Li, B. G., and Piao, S. L.: High-resolution mapping of combustion processes and implications for CO<sub>2</sub> emissions, *Atmos. Chem. Phys.*, 13, 5189–5203, <https://doi.org/10.5194/acp-13-5189-2013>, 2013.
- Wang, G., Huang, L., Gao, S., Gao, S., and Wang, L.: Characterization of water-soluble species of PM<sub>10</sub> and PM<sub>2.5</sub> aerosols in urban area in Nanjing, China, *Atmos. Environ.*, 36, 1299–1307, 2002.
- Wang, G., Wang, H., Yu, Y., Gao, S., Feng, J., Gao, S., and Wang, L.: Chemical characterization of water-soluble components of PM<sub>10</sub> and PM<sub>2.5</sub> atmospheric aerosols in five locations of Nanjing, China, *Atmos. Environ.*, 37, 2893–2902, 2003.
- Wang, T., Cheung, V. T. F., Anson, M., and Li, Y. S.: Ozone and related gaseous pollutants in the boundary layer of eastern China: overview of the recent measurements at a rural site, *Geophys. Res. Lett.*, 28, 2373–2376, 2001.
- Wang, T., Wong, C. H., Cheung, T. F., Blake, D. R., Arimoto, R., Baumann, K., Tang, J., Ding, G. A., Yu, X. M., Li, Y. S., Streets, D. G., and Simpson, I. J.: Relationships of trace gases and aerosols and the emission characteristics at Lin'an, a rural site in eastern China, during spring 2001, *J. Geophys. Res.*, 109, D19S05, <https://doi.org/10.1029/2003JD004119>, 2004.
- Wang, Y., Ying, Q., Hu, J., and Zhang, H.: Spatial and temporal variations of six criteria air pollutants in 31 provincial capital cities in China during 2013–2014, *Environ. Int.*, 73, 413–422, 2014.
- Wang, Y. Q., Zhang, X. Y., Arimoto, R., Cao, J. J., and Shen, Z. X.: The transport pathways and sources of PM<sub>10</sub> pollution in Beijing during spring 2001, 2002 and 2003, *Geophys. Res. Lett.*, 31, L14110, <https://doi.org/10.1029/2004GL019732>, 2004.
- Wu, J., Xu, C., Wang, Q., and Cheng, W.: Potential sources and formations of the PM<sub>2.5</sub> pollution in urban Hangzhou, *Atmosphere*, 7, 100, <https://doi.org/10.3390/atmos7080100>, 2016.
- Wu, Y., Hu, M., Zeng, L., Dong, H., Li, X., Lu, K., Lu, S., Yang, Y., and Zhang, Y.: Seasonal variation of trace gas compounds and PM<sub>2.5</sub> observed at an urban supersite in Beijing, EGU General Assembly, Vienna, Austria, 17–22 April 2016, EPSC2016-12409, 2016.
- Xu, Z., Wang, T., Xue, L. K., Louie, P. K. K., Luk, C. W. Y., Gao, J., Wang, S. L., Chai, F. H., and Wang, W. X.: Evaluating the uncertainties of thermal catalytic conversion in measuring atmospheric nitrogen dioxide at four differently polluted sites in China, *Atmos. Environ.*, 76, 221–226, 2013.
- Xue, L. K., Wang, T., Gao, J., Ding, A. J., Zhou, X. H., Blake, D. R., Wang, X. F., Saunders, S. M., Fan, S. J., Zuo, H. C., Zhang, Q. Z., and Wang, W. X.: Ground-level ozone in four Chinese cities: precursors, regional transport and heterogeneous processes, *Atmos. Chem. Phys.*, 14, 13175–13188, <https://doi.org/10.5194/acp-14-13175-2014>, 2014a.
- Xue, L. K., Wang, T., Louie, P. K. K., Luk, C. W. Y., Blake, D. R., and Xu, Z.: Increasing external effects negate local efforts to control ozone air pollution: a case study of Hong Kong and implications for other Chinese cities, *Environ. Sci. Technol.*, 48, 10769–10775, 2014b.
- Yang, L. X., Cheng, S. H., Wang, X. F., Nie, W., Xu, P. J., Gao, X. M., Yuan, C., and Wang, W. X.: Source identification and health impact of PM<sub>2.5</sub> in a heavily polluted urban atmosphere in China, *Atmos. Environ.*, 75, 265–269, 2013.

- Yu, S. C., Zhang, Q. Y., Yan, R. C., Wang, S., Li, P. F., Chen, B. X., Liu, W. P., and Zhang, X. Y.: Origin of air pollution during a weekly heavy haze episode in Hangzhou, China, *Environ. Chem. Lett.*, 12, 543–550, 2014.
- Zhang, H. L., Li, J. Y., Ying, Q., Yu, J. Z., Wu, D., Cheng, Y., He, K. B., and Jiang, J. K.: Source apportionment of PM<sub>2.5</sub> nitrate and sulfate in China using a source-oriented chemical transport model, *Atmos. Environ.*, 62, 228–242, 2012.
- Zhang, L. M., Gong, S. L., Padro, J., and Barrie, L.: A size segregated particulate dry deposition scheme for an atmospheric aerosol module, *Atmos. Environ.*, 35, 549–560, 2001.
- Zhang, R., Jing, J., Tao, J., Hsu, S.-C., Wang, G., Cao, J., Lee, C. S. L., Zhu, L., Chen, Z., Zhao, Y., and Shen, Z.: Chemical characterization and source apportionment of PM<sub>2.5</sub> in Beijing: seasonal perspective, *Atmos. Chem. Phys.*, 13, 7053–7074, <https://doi.org/10.5194/acp-13-7053-2013>, 2013.
- Zhang, R. Y., Suh, I., Zhao, J., Zhang, D., Fortner, E. C., Tie, X. X., Molina, L. T., and Molina, M. T.: Atmospheric new particulate formation enhanced by organic acids, *Science*, 304, 1487–1490, 2004.
- Zhang, Q., Yuan, B., Shao, M., Wang, X., Lu, S., Lu, K., Wang, M., Chen, L., Chang, C.-C., and Liu, S. C.: Variations of ground-level O<sub>3</sub> and its precursors in Beijing in summertime between 2005 and 2011, *Atmos. Chem. Phys.*, 14, 6089–6101, <https://doi.org/10.5194/acp-14-6089-2014>, 2014.
- Zhang, Q., Streets, D. G., Carmichael, G. R., He, K. B., Huo, H., Kannari, A., Klimont, Z., Park, I. S., Reddy, S., Fu, J. S., Chen, D., Duan, L., Lei, Y., Wang, L. T., and Yao, Z. L.: Asian emissions in 2006 for the NASA INTEX-B mission, *Atmos. Chem. Phys.*, 9, 5131–5153, <https://doi.org/10.5194/acp-9-5131-2009>, 2009.
- Zhong, Q. R., Huang, Y., Shen, H. Z., Chen, Y. L., Chen, H., Huang, T. B., Zeng, E. Y., and Tao, S.: Global estimates of carbon monoxide emissions from 1960 to 2013, *Environ. Sci. Pollut. R.*, 24, 864–873, 2014.